CERN-LHCC-2014-020
TOTEM-TDR-002
15 September 2014

TOTEM

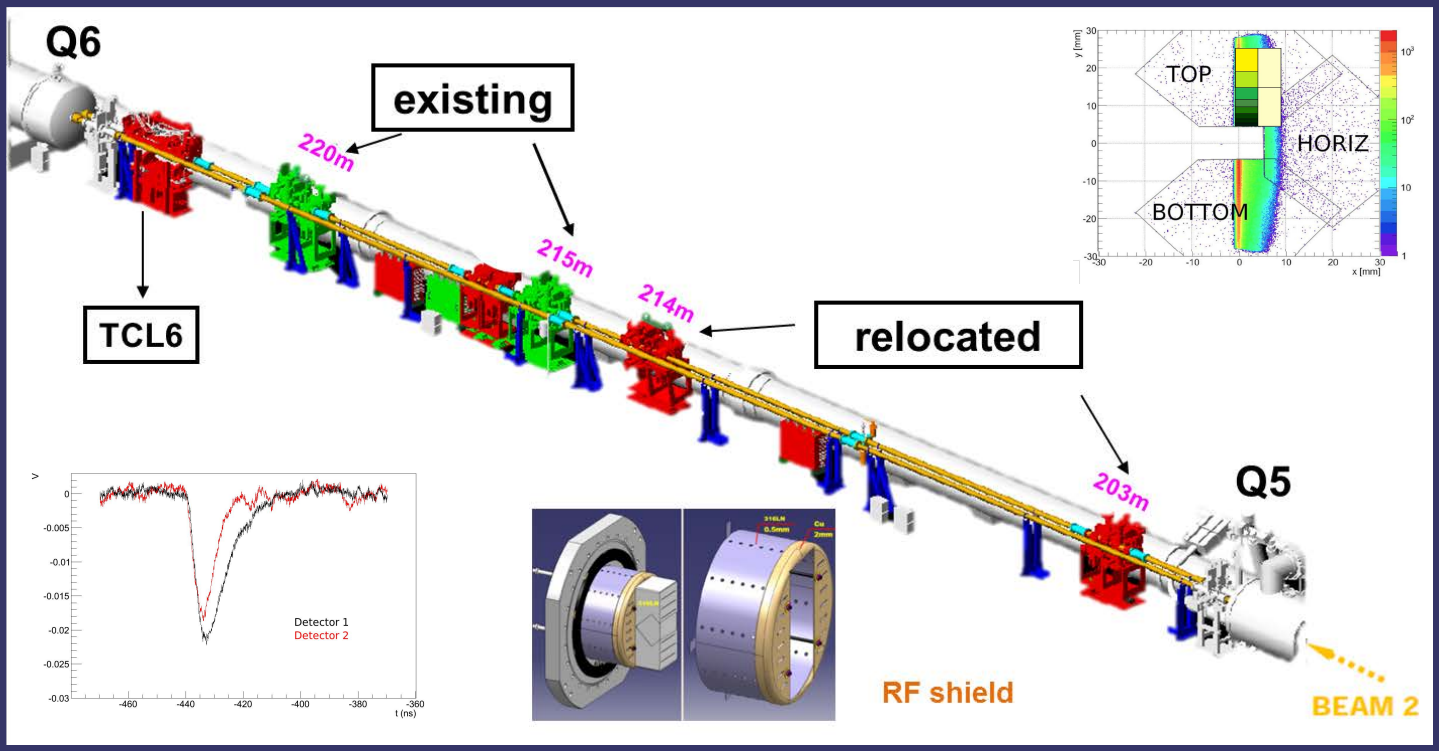

Timing Measurements in the Vertical Roman Pots of the TOTEM Experiment Technical Design Report

TOTEM-2014-003

CERN-LHCC-2014-020, TOTEM-TDR-002
September 2014

Technical Design Report

Timing Measurements in the Vertical Roman Pots of the TOTEM Experiment

The TOTEM Collaboration

Abstract

The TOTEM upgrade programme focusses on improving the experiment's capability to explore and measure new physics in Central Diffractive processes in two complementary projects, both based on the installation of proton-time-of-flight detectors in Roman Pots to reconstruct the longitudinal vertex position and thus to assign the proton vertex to the correct central CMS tracker vertex in the presence of event pileup. The present TDR discusses the instrumentation developments, physics potential and performance for operation with a $\beta^* =$ 90 m beam optics, for which the vertical Roman Pots will be equipped with timing detectors with $\sim$ 50ps resolution. In this scenario, the leading proton acceptance covers all diffractive masses, provided that the protons' four-momentum transfer $|t| > \sim 0.01$ GeV^2. In a complementary way, the second project, the CMS-TOTEM Precision Proton Spectrometer (CT-PPS) for standard LHC fills at low β^* targeting processes with high diffractive masses (> 300 GeV/c^2) and leading protons in the horizontal Roman Pots is described in another TDR.

Contents

1 Introduction **3**

2 Physics Motivation and Program **5**
2.1 Physics motivation 5
2.2 Physics program 6
2.2.1 Low mass resonances and glueball states in central diffraction 6
2.2.2 Exclusive central diffractive $c\bar{c}$ production 7
2.2.3 Search for missing mass and momentum candidates 8
2.2.4 (Exclusive) central diffractive jet production 9

3 Running Scenario **11**
3.1 Pileup at $\beta^* = \mathbf{90}\,\mathrm{m}$ 11
3.2 Luminosity reach at $\beta^* = \mathbf{90}\,\mathrm{m}$ 12
3.3 Commissioning and start-up strategy 13

4 Physics and Detector Performance **15**
4.1 Tracking detectors 15
4.1.1 Roman Pots 15
4.1.2 CMS Tracker 17
4.1.3 Combined CMS and TOTEM detectors 19
4.2 Timing detectors 22
4.2.1 Optimization for physics signal and background rates 22
4.2.2 Trigger strategy 26

5 Timing Detector System **29**
5.1 Timing detectors 29
5.1.1 Detector segmentation 29
5.1.2 Readout electronics 30
5.2 Clock distribution 34
5.2.1 Transmission Unit 35
5.2.2 Distribution Unit 36
5.2.3 Measurement Unit 36
5.2.4 Receiving Unit 36

6 Costs and Schedule **38**
6.1 Costs 38
6.2 Schedule 39

1 Introduction

The TOTEM experiment has measured elastic [1], total [2, 3, 4, 5], inelastic [5, 6] and diffractive [7] cross sections, as well studied the charged particle pseudorapidity density $dN_{ch}/d\eta$ [8], at energies so far explored during the LHC running. TOTEM has also measured $dN_{ch}/d\eta$ together with the CMS experiment [9], including single, double and central diffraction topologies using the forward inelastic detectors in combination with one of the large LHC detectors, as originally proposed at the time of the TOTEM TDR [10].

While the measurement of the total cross section and the elastic scattering can be performed using only the TOTEM detectors, the CMS/TOTEM experiment offers the prospect of more detailed studies of diffractive events with an unprecedented particle coverage over 15 units of rapidity, that extends further down to production angles of a few micro-radians with the measurement of very forward protons.

The future physics program of TOTEM includes the physics cases and analysis channels outlined in the following sections, which exploit the LHC as a pure gluon-gluon collider in particular via central diffractive production. The relevant analysis channels have already been explored and tested with the data available from the July 2012 runs. The required statistics and consequent integrated luminosity for 2015 and 2016 are derived from the extrapolation of the current data analyses, where the physics observables and results were extracted from the data taken with $\beta^* = 90\,\text{m}$.

The goals of our future physics programme, that will be discussed later in more detail, are summarized as shown in Table 1.

To further extend the measurement potentialities for the experiment at luminosities where the pile-up and multiple tracks in the proton detectors make it difficult to identify and disentangle real diffractive events from other event topologies, TOTEM has proposed [11] to add a timing measurement capability to measure the time-of-flight difference between the two outgoing protons. This yields the longitudinal vertex position z_{pp} with a precision of a few cm if they come from the same collision. The protons vertex has then to be matched with the $z_{central}$ of the central event reconstructed by CMS. A R&D program on timing detectors, presented in detail in the following pages, is well under way and now in its final phase.

To mitigate the problem of multi-track reconstruction ambiguities from only two detectors' projections, the RP stations removed from the 147 m locations have been reinstalled at 210 m, with one of the two units rotated azimuthally (i.e. tilted around the beam axis) by 8^o. At a later stage the strip detectors in the tracking pots will be replaced with radiation-hard pixel detectors (using new tracking detectors based on 3D pixel technology).

The TOTEM triggers, combining information from the inelastic detectors and the silicon detectors in the RP stations located at 220 m downstream from the Interaction Point (IP), can be used by the general CMS trigger scheme and combined with other CMS triggers. The digitization of the TOTEM detectors and the data acquisition system are both fully compatible with the CMS DAQ, thus enabling a common read-out of both detectors while maintaining a stand-alone read-out for TOTEM.

Furthermore, operation at highest luminosities requires some technical adaptations to the detector housing in view of impedance reduction.

Table 1: *Overview of physics program goals for the 2015 and 2016 data taking period.*

2015

***** Low-mass diffractive spectroscopy *****		
Past Luminosity:	$\sim 0.003\,\mathrm{pb}^{-1}$	~ 3 bunches, $\mu = 5\%$, ~ 1 physics-day
Requirement:	factor $\sim 300 \rightarrow \mathbf{1\,pb^{-1}}$	
Solution:	~ 1000 bunches, ~ 1 physics-day	or ~ 100 bunches, ~ 10 physics-days
Notes: do-able even without crossing-angle if problems.		
***** Glueball searches and exclusive χ_c production *****		
Past Luminosity:	$\sim 0.003\,\mathrm{pb}^{-1}$	~ 3 bunches, $\mu = 5\%$, ~ 1 physics-day
Requirement:	factor $\sim 3000 \rightarrow \mathbf{10\,pb^{-1}}$	
Solution:	~ 1000 bunches, ~ 10 physics-days	
Notes: needed $\mu \sim 10\%$ (timing detectors already useful if available).		

2016

***** Missing mass searches, gluonic states BR/couplings, ***** **Exclusive dijet production, hard-diffraction**		
Past Luminosity:	$\sim 0.1\,\mathrm{pb}^{-1}$	~ 100 bunches, $\mu = 5\%$, ~ 1 physics-day
Requirement:	factor $\sim 1000 \rightarrow \mathbf{100\,pb^{-1}}$	
Solution:	~ 1000 bunches, ~ 10 physics-days,	$\mu \sim 50\%$
Notes: needed timing detectors in vertical RPs.		

* These figures contain implicit assumptions of a DAQ consolidation (standalone and within CMS) and of trigger rates' reduction feasible at L1 or at HLT.

2 Physics Motivation and Program

2.1 Physics motivation

The consolidation program of TOTEM [11] focuses on improving its capabilities to measure Central Diffractive (CD) processes, $p + p \to p \oplus X \oplus p$, in special high β^* optics runs with common data taking with CMS. The combination of the CMS and TOTEM experiments gives an exceptionally large pseudorapidity coverage for tracking and calorimetry that is well suited for studies of diffractive processes like CD [12]. The addition of timing sensors with ~ 50 ps timing resolution in the vertical Roman Pots (RP) allows access to CD processes with O(pb) cross-sections. This enables important tests of Quantum Chromo-Dynamics (QCD) predictions, unique measurements of subtle QCD effects as well as even searches for possible new physics that might have escaped the standard LHC searches.

In CD reactions, also called Double Pomeron Exchange (DPE), the protons stay intact and "rapidity gaps", regions without primary particle production (indicated by $\oplus$), are formed between the protons and the state X. In these events, the four-momentum of X can both be measured by the main central detector and calculated from the measurement of the two scattered protons in the RP's. In this way CD events resemble more electron-positron annihilation events than normal parton-parton scattering events at LHC, where the initial state of the interacting partons is not well known since the proton remnants cannot be measured accurately. In CD reactions, the mass of X, M_X, can be reconstructed from the fractional momentum loss, ξ, of the scattered protons by $M_X = M_{pp} \sim \sqrt{\xi_1 \xi_2 s}$. If the state X is a well-defined state, like a particle or a fixed number of particles or jets, then the process is called "exclusive". In exclusive CD reactions, to a very good approximation, the final state X obeys a $J_z = 0$, C-even, P-even, selection rule [13]. Here J_z is the projection of the total angular momentum along the proton beam axis.

CD is a t-channel exchange process, and the absolute value of the four-momentum-transfer squared, $|t|$, follows an approximately exponentially decreasing distribution. The carriers of this t-channel exchange are either a system of gluons g (with neutral colour) or photons γ. The leading order description of this colour-singlet gluon system is called the Pomeron $\mathbb{P}$. In CD processes, the dominant contribution comes from $\mathbb{P}$ $\mathbb{P}$scattering complemented by "photoproduction" i.e. $\mathbb{P}\gamma$ fusion.

In $\beta^* = 90$ m optics runs, protons with any ξ can be detected in the vertical RPs and hence, in CD reactions, any M_X, as long as the $|t|$ of both scattered protons is larger than ~ 0.04 GeV^2. This is complementary to the reach of the CMS-TOTEM precision proton spectrometer (CT-PPS) [14] that only has access to $M_X \gtrsim 300$ GeV/c^2 and aims to measure processes with O(fb) cross-sections in normal high-luminosity running. In addition, pile-up, multiple pp interactions per bunch crossing, is much less of a problem in high β^* runs with an average number of inelastic pp events per bunch crossing, $\mu \lesssim 1$, compared to $\mu \gtrsim 25$ in normal high-luminosity LHC runs. The excellent pseudorapidity coverage of CMS and TOTEM allows, in addition to the comparison between the central mass, $M_{central}$, computed from the particle flow objects and M_X, to compare the transverse (p_T) and longitudinal (p_z) momentum of the central state and the two protons as well as verify the rapidity gaps predicted by the proton ξ measurements.

The physics topics covered by measurements of CD processes in high β^* runs include spectroscopy of CD produced low mass resonances and glueball states, studies of the rapidity gap survival probability as well as searches for new physics in CD reactions via missing mass or momentum signature. In addition, one can extract an ultra-pure gluon jet sample to study the properties of gluon jets. Below follows a more detailed description of the CD processes of interest. In most cases, a preliminary analysis has already been performed on the data of the common CMS-TOTEM $\beta^* = 90$ m run at $\sqrt{s} = 8$ TeV in July 2012 showing the feasibility of the measurements outline below. The available double arm RP (jet and lepton) triggered sample corresponds

to an integrated luminosity of $\sim$0.003 ($\sim$0.1) pb^{-1}. In addition to CD processes, also several single diffractive (SD) processes can be studied in detail with proton tagging like SD dijet, J/Ψ and W production in $\sim$10 pb^{-1} as well as SD Z production in $\sim$100 pb^{-1} of integrated $\beta^* = 90$ m luminosity.

2.2 Physics program

2.2.1 Low mass resonances and glueball states in central diffraction

The CD process effectively turns LHC into a gluon-gluon collider and provides an excellent opportunity to study gluon systems with a longitudinal momentum fraction $x \sim 10^{-4}$ and, in particular, to search for glueball candidates. Glueballs are predicted by QCD as bound gluon states with no valence quark content. QCD lattice calculation foresee a $J^{PC} = 0^{++}$ ground state and a 2^{++} state followed by a spectrum of excited states [15, 16]. Scalar and tensorial f states in the 1.5 to 2.5 GeV mass region are generally regarded as potential glueball candidates. The absence of valence quarks, in combination with the $J_z^{PC} = 0^{++}$ selection rule, makes exclusive CD reactions an ideal place to search for them. The hypothesis, whether a resonance is a glueball or not, can be studied by measuring its exclusive CD production cross-section as well as its decay modes and their branching ratios [15, 17].

The mass distribution for exclusive CD $\pi^+\pi^-$ events up to a few GeV has been measured at lower center-of-mass energies [18, 19, 20, 21] and in fixed target experiments [22]. Due to limited mass resolution or, in the absence of proton tagging, due to significant backgrounds, deconvolution techniques have usually been applied to extract information about the resonance production. In the case of CMS-TOTEM, the excellent mass resolution ($\sim$ 20-30 MeV) with the tracker for charged-particle-only final states, in combination with the proton tagging, allows clearly to identify the produced resonances without further steps and even to extend the analysis to four particle final states like $\rho^0\rho^0$ and $\eta\eta$. In the case of η, the soft γ in the $\eta \to \pi^+\pi^-\gamma$ decay is assumed to escape detection.

First, events with two RP protons and only two or four charged particles in the tracker with a zero net charge are selected in the double arm RP triggered sample. Then, p_T compatibility between the central and pp systems as well as $\xi \sim 0$ compatibility for the protons (resulting effectively in a $M_X \lesssim 10$ GeV selection) is required. The background has been shown to be low by selecting events with the same criteria but with a non-zero sum of the charges for the particles in the tracker. In the analyzed data sample of $\sim$3 nb^{-1}, about 1000 $\pi^+\pi^-$ and a few tens of $\rho\rho$ and $\eta\eta$ exclusive candidates were found, where for the latter the two $\pi^+\pi^-$ combinations are required to be compatible either both with the ρ or both with the η mass.

With increased statistics, the analysis will be extended to at least six and eight charged particle final states. The particle identification with the tracker dE/dx at the p_T's typical for the decay products of these low mass resonances allows to confirm the $\pi^\pm$ hypothesis or in the case of K$^\pm$ select a clean K$^+$K$^-$ sample. The spin of the produced resonance can be determined by analyzing either the decay distribution of final state particles/resonances or the azimuthal angle difference $\Delta\phi$ of the two scattered protons. The sensitivity to the spin of the produced state of the methods has been confirmed on the available data set.

To unambiguously determine the spin of the CD produced resonances as well as provide first cross-section$\times$branching ratio estimates for the final states mentioned, the current statistics of double arm RP triggered events should be increased by a factor $\sim$300 corresponding to $\sim$1 pb^{-1} of integrated luminosity. This will, in addition, allow for a first determination of the P_T spectra in exclusive CD production for each identified resonance. These measurements will reveal important information about gluon systems at low x-values and the nature of the soft Pomeron. On the other hand, for precise cross-section$\times$branching ratio estimates that are needed for the glueball candidate analysis as well as the observation of resonances in six and eight charged particle final

states, the current sample of double arm RP triggered events should be increased by a factor ∼3000 corresponding to ∼10 pb^{-1} of integrated luminosity.

2.2.2 Exclusive central diffractive $c\bar{c}$ production

In recent years there has been an increased interest to measure exclusive CD production of $c\bar{c}$ mesons. In fact, exclusive production of $c\bar{c}$ states, and, especially, of χ_c is regarded as an excellent laboratory to study QCD and the role of the Pomeron, particularly since the mass of the central system is high enough to allow the use of perturbative QCD [23, 24]. The leading order diagram for exclusive χ_c production in perturbative QCD is through a t-channel two-gluon exchange as shown in Figure 1 (left). Exclusive χ_c production has been observed by both CDF [25] and LHCb [26]. These observations are based on the J/$\Psi\gamma$ decay mode, where the separation between the different χ_c states is difficult due to the limited energy resolution for the γ in the experiments. In addition, the more precise measurement from LHCb suffers from proton dissociation background.

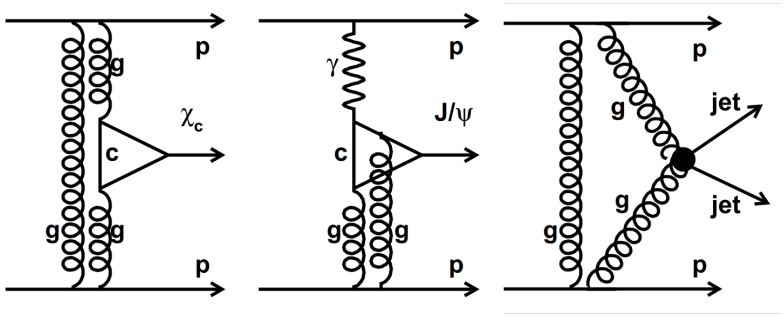

Figure 1: *Leading order diagrams for exclusive central diffractive χ_c (left), J/Ψ (middle) and dijet production (right) in pp collisions.*

With CMS-TOTEM, the different χ_c state can easily be separated in charged-particle-only final states and the proton dissociation background can be elimated using proton tagging. The available data set contains a few χ_c exclusive candidates in such final states, consistent with CDF and LHCb measurements. For good determination of the cross-section×branching ratio in χ_c decays to charged-particle-only final states, the current statistics of double arm RP triggered events should be increased by a factor ∼3000 corresponding to ∼10 pb^{-1} of integrated luminosity. This will allow to significantly improve the experimental data on exclusive χ_c production and test model predictions [27].

In addition to χ_c, exclusive J/Ψ and $\Psi(2s)$ production [28, 29] as well as exclusive double charmonium production [30] has been observed at LHC in the $\mu^+\mu^-$ decay mode. Exclusive J/Ψ and $\Psi(2s)$ production is mainly due to photoproduction, see Figure 1 (middle). A measurement allows to extract the photoproduction cross-section versus the center-of-mass energy of the photon-proton system to be compared to the corresponding HERA measurement. All of the existing measurements suffer from proton dissociation backgrounds. Extrapolating from the measured cross-section by LHCb, the current sample of lepton triggered events should be increased by a factor ∼1000 corresponding to ∼100 pb^{-1} of integrated luminosity for CMS-TOTEM to be able to make such a measurement with proton tagging. Proton tagging also allows cleanly to determine the P_T spectrum of the produced J/Ψ meson, even at larger P_T's, where proton dissociation events dominate the existing measurements. The Odderon, the C-odd partner of the Pomeron, is predicted to significantly modify the large P_T part of the spectrum [31], which a CMS-TOTEM measurement could test. Up to now there is no compelling experimental evidence of the existence of Odderon exchange despite being predicted by QCD.

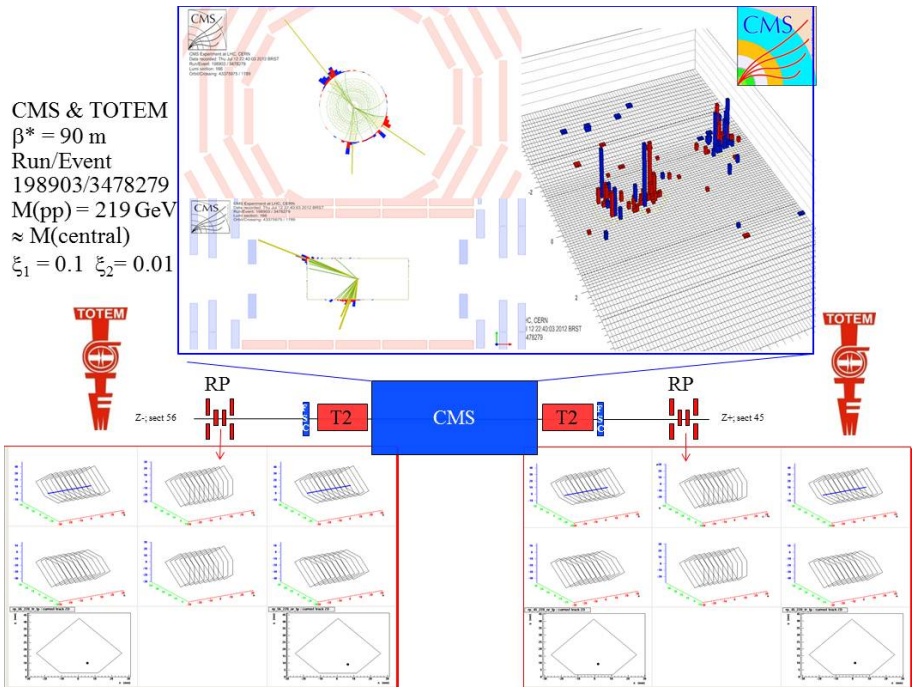

Figure 2: *A central diffractive three-jet event recorded by TOTEM and CMS in a $\beta^* = 90$ m run at $\sqrt{s} = 8$ TeV. The upper part of the figure displays the central part of the event, as seen in CMS; the lower part displays the proton information in the TOTEM Roman Pots.*

2.2.3 Search for missing mass and momentum candidates

CD allows to measure simultaneously the initial and final state kinematics precisely, which can be used to search for events with missing mass or missing momentum signature. This opens up ways to search for new physics that might have escaped the searches of the general purpose detectors, CMS and ATLAS, e.g. in scenarios where the new physics couples dominantly or only to gluons. A preliminary search for such events has been performed on the existing data samples of double arm RP triggered and jet triggered events [32]. Only CD events with a central mass, $M_{central}$, less or equal to M_X are examined to avoid contamination from pileup events. $M_{central}$ is reconstructed from the sum of the CMS particle flow objects and the missing momentum, $\not{p}$, is reconstructed from the difference of the sum of the proton momenta and the sum of the momenta of the particle flow objects. The rapidity gaps, $\Delta\eta = -ln\xi$, predicted by the proton ξ measurements are verified using the T2 detectors with a rapidity coverage of $5.3 < |\eta| < 6.5$. To probe O(pb) cross-sections for the two signal topologies described below, a statistics of double arm RP triggered and of jet triggered events corresponding to an integrated luminosity of ~ 100 pb^{-1} is needed.

To verify the performance and the search methodology, control samples of events were selected both in double arm RP triggered sample and in the jet triggered sample with the following requirements: charged particles in T2, when allowed by the rapidity gaps predicted by the ξ measurements, and no charged particles in T2, when not allowed by the rapidity gaps predicted by the ξ measurements. Many such events, corresponding to standard CD events, were found in both the double arm RP triggered and jet triggered data samples and these events will be used for a determination of the inclusive CD event and CD jet cross-sections, respectively. One such candidate in the jet sample with $M_{central} \approx M_X$ is shown in Figure 2.

A first signal topology, depicted schematically in Figure 3(a), are events with charged particles in T2 violating the ξ predicted rapidity gaps. This could happen if a particle is created in the CD reaction and some of its decay products go into the T2 η acceptance region. Such events would be

used searching for the production of new particles by studying the M_X (and $M_X - M_{central}$) distributions. No candidate events were found in the available jet sample. Remaining single diffractive pileup and beam halo background makes the double armed RP triggered sample unusable for such searches.

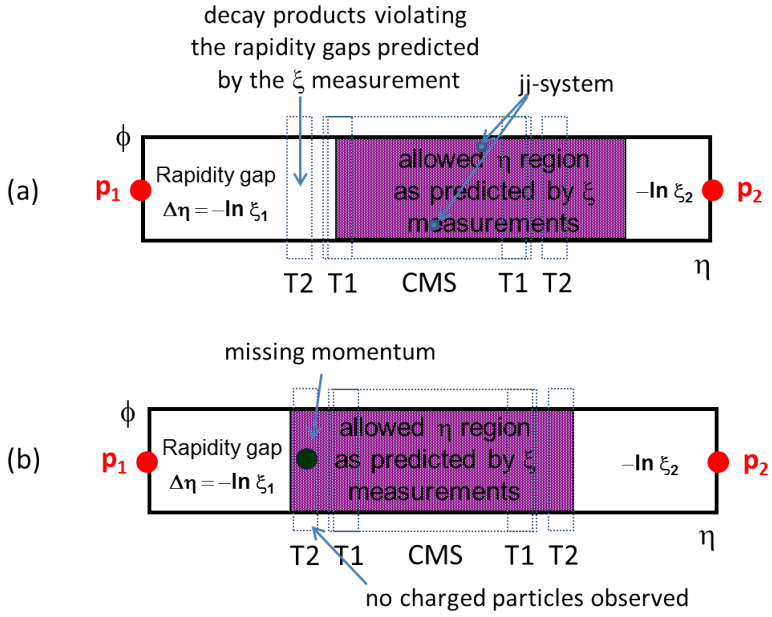

Figure 3: *Schematical drawings of the two event topologies used in the search for missing mass and momentum signatures in CD events. (a) Events with charged particles in T2, violating the rapidity gaps predicted by the ξ measurement, from e.g. the decay of a CD produced particle. (b) Events with high missing momentum, pointing towards an η region with good CMS-TOTEM instrumentation and no charged particles or energy deposites are observed in the η region where the missing momentum points. T2 η region given as example. Could be due to a CD produced particle escaping undetected.*

A second even more striking signature is to search for events with high missing momentum pointing towards the region with good CMS-TOTEM instrumentation ($|\eta| < 6.5$) and not observing charged particles or energy deposites in the η region close to where the missing momentum points. Figure 3(b) depicts the case where the missing momentum points towards T2. This could happen if a particle is created in the CD reaction and escape the experimental apparatus undetected in the T2 acceptance region. Events are rejected if more forward rapidity gaps than T2 ($|\eta| < 6.5$) would be allowed by the ξ measurements. Events with missing mass up to 400 GeV were found in both the double arm RP and jet triggered data set with background events expected from neutral particles escaping detection in the T2 acceptance region, due to "acceptance gaps" between the forward detectors as well as from $p + p \to N^* \oplus X \oplus p$ or $p \oplus X \oplus N^*$ reactions. In the latter case, one of the observed protons would come from a decay of a nucleon resonance, N^*, and the other decays products of the N^* would escape detection. With increased statistics, its is expected that these backgrounds will be modelled sufficiently well.

2.2.4 (Exclusive) central diffractive jet production

In exclusive jet production both protons escape intact the hard interaction, and only a two- or three-jet system is centrally produced, $p + p \to p \oplus jj, jjj \oplus p$. Exclusive production may occur through a t-channel two-gluon change at leading order in perturbative QCD as shown schematically in

Figure 1 (right). Exclusive dijet production in hadronic collisions was first observed at the Tevatron [33]. Most events with two scattered protons and central jets will not be exclusive $X = j + j$ or $j + j + j$, but will have additional particle production from the Pomeron remnants. These will be referred to as CD jet production. Exclusive may be regarded as a particular case of CD jet production with only the jets in the final state, and no Pomeron remnants. In high β^* runs, CMS-TOTEM can study CD dijets with $E_T > 20$ GeV at any M_X. This is complementary to the CT-PPS [14] acceptance in standard LHC running, which has access only to $M_X \gtrsim 300$ GeV/c^2 .

Theoretically, exclusive dijets should be pure gluon jets $\sim 99\%$ of the time [13], a unique situation which can be exploited for studying jet fragmentation. The LHC is then used as a "gluon jet factory". Light-quark dijets should be suppressed approximately as $(m(q)/m(jj))^2$ according to the $J_z = 0$ rule [13] when $t_1 \sim t_2 \sim 0$. Exclusive three-jet events can be both ggg and $q\bar{q}g$. In the $q\bar{q}g$ case we expect a democratic population of quark flavours (except top): $\sigma(u\bar{u} = d\bar{d} = s\bar{s} = c\bar{c} = b\bar{b})$. The kinematic distributions of the three jets are expected to be different for ggg and $q\bar{q}g$, with $q\bar{q}g$ events being more "Mercedes-like" [34], another prediction of QCD that can be tested.

Some two- and three-jet events, though not exclusive since $M(jj, jjj) \ll M(pp)$, were already seen by CMS and TOTEM during the short high β^* run in July 2012. Common data were recorded with a CMS trigger on two jets with $E_T > 20$ GeV. Selecting events with a proton in each direction in the TOTEM Roman Pots, extremely clean events with jets were found, as shown in Figure 2.

Exclusive CD jet production will shed light on a number of crucial aspects of the proton structure and the strong interaction. On the one hand, the two-gluon proton vertex measures the (skewed) unintegrated gluon parton distribution function of the proton. On the other hand, the experimental study of the rapidity gap survival probability opens up a new window on the study of soft multiple parton interactions. With 100 pb^{-1} of high β^* running, we expect a sample of about 10000 exclusive CD jet events with $M_X > 60$ GeV, since the expected visible cross-section for CMS-TOTEM is about 100 pb [35]. The obtained sample will enable studies of the azimuthal difference $\Delta\phi$ between the scattered protons, the shape of the proton t distribution and the overall cross section behaviour with M_X, providing a good test of different models [35, 36]. In addition with an integrated luminosity of ~ 100 pb^{-1}, a study of the γ-jet/dijet ratio vs M_X to deduce the resolved hard Pomeron quark content (e.g. d/u ratio) [37] could be performed.

3 Running Scenario

TOTEM will operate in a wide range of luminosities giving access to cross-sections from 100 mb down to the fb level. A rough overview is given in Table 2 [11].

Table 2: *Overview of expected running scenarios at $\sqrt{s} = 13\,TeV$, with their respective ranges of inelastic pileup μ and delivered luminosity. The precise values depend on the bunch size, the number of bunches, and the emittance.*

β^* [m]	cr. angle [μrad]	ε_N [μm rad]	N [10^{11} p/b.]	k bunches	μ	Luminosity [$\mathrm{cm^{-2}\,s^{-1}}$]	
2500	0	2	$0.7 \div 1.5$	2	$0.004 \div 0.02$	$(1.2 \div 5.6) \times 10^{27}$	$= (0.1 \div 0.5)\,\mathrm{nb^{-1}/24h}$
90	0	2	$0.5 \div 1.5$	156	$0.06 \div 0.5$	$(1.3 \div 12) \times 10^{30}$	$= (0.1 \div 1)\,\mathrm{pb^{-1}/24h}$
90	100	2	$0.5 \div 1.5$	1000	$0.06 \div 0.5$	$(0.9 \div 7.7) \times 10^{31}$	$= (0.8 \div 7)\,\mathrm{pb^{-1}/24h}$
0.5	$310 \div 390$	$1.9 \div 3.75$	1.15	$2520 \div 2760$ ($\Delta t = 25\,$ns)	$19 \div 34$	$(0.8 \div 1.3) \times 10^{34}$	$= (0.7 \div 1.1)\,\mathrm{fb^{-1}/24h}$

Large cross-section phenomena (elastic scattering at low $|t|$, minimum-bias physics, soft diffraction) are covered by the high-β^* scenarios with 2 to 156 bunches. Passing on to detailed studies of central diffraction, in particular hard or exclusive processes, one is confronted with much lower cross-sections, well below 1 mb, and thus with the challenge to find a balance between achieving the required luminosity and suppressing the background created by event pileup. First measurements in July 2012 based on a special run with the $\beta^* = 90\,$m optics showed that already an inelastic pileup level of $\mu \sim 5\,\%$ led to difficulties in selecting clean samples of central diffractive events. At the same time, statistics suffered from the low luminosity of about $10^{30}\,\mathrm{cm^{-2}s^{-1}}$.

High-mass central diffraction (with $M > 250\,$GeV) can be covered by continuously operating horizontal Roman Pots, equipped with timing detectors, in standard low-β^* fills. This part of the upgrade program is pursued in the framework of the CMS TOTEM Precise Proton Spectrometer collaboration (CT-PPS). It is described in a dedicated TDR [14] and it is not subject of the present document.

On the other hand, low-mass central diffractive events are excluded from this low-β^* program due to lacking detector acceptance. For this physics the $\beta^* = 90\,$m optics is ideal, given its acceptance for all diffractive masses via the vertical RPs. The following sections will outline the strategy for increasing the luminosity, while keeping the pileup at an acceptable level.

3.1 Pileup at $\beta^* = 90\,$m

Table 3 and Figure 4 show the mean number of inelastic interactions per bunch crossing, μ, and the conditional pileup probability, $P(n > 1)/P(n > 0)$ (where n is the number of interactions in a bunch crossing and $P(n)$ is its Poissonian probability), for $\beta^* = 90\,$m as a function of the bunch population N.

The quantity $P(n > 1)/P(n > 0)$ is a figure of merit for the pileup contamination of the data. In the first running period after LS1, before the installation of timing detectors, this contamination should stay at a manageable level, i.e. not much higher than 5%. On the other hand, both for the ease of LHC operation and for maximisation of the luminosity, the bunch population N should be as close as possible to the nominal 1.15×10^{11}. A good compromise lies in the range $(0.6 \div 0.7) \times 10^{11}$. For a given optics and emittance, and with limited bunch population, the only way of increasing the luminosity is to maximise the number of bunches. Later, with timing detectors, disentangling pileup events by vertex reconstruction will become possible and will allow bunch

populations up to the technical LHC limit, currently expected to be at 1.5×10^{11}.

Table 3: *Luminosity per colliding bunch pair, $\mathscr{L}_{bb}$, mean number of inelastic interactions per bunch crossing, μ, and conditional pileup probability, $P(n>1)/P(n>0)$, for $\beta^* = 90\,m$, $\sqrt{s} = 13\,TeV$ and emittance $\varepsilon_N = 2\,\mu m\,rad$, as a function of the bunch population N.*

N [10^{11}]	$\mathscr{L}_{bb}$ [cm^{-2}s^{-1}]	μ	$\frac{P(n>1)}{P(n>0)}$
0.4	5.5×10^{27}	0.042	0.021
0.5	8.6×10^{27}	0.065	0.032
0.6	1.2×10^{28}	0.094	0.047
0.7	1.7×10^{28}	0.13	0.064
0.8	2.2×10^{28}	0.17	0.077
1.15	4.6×10^{28}	0.34	0.16
1.5	7.8×10^{28}	0.59	0.27

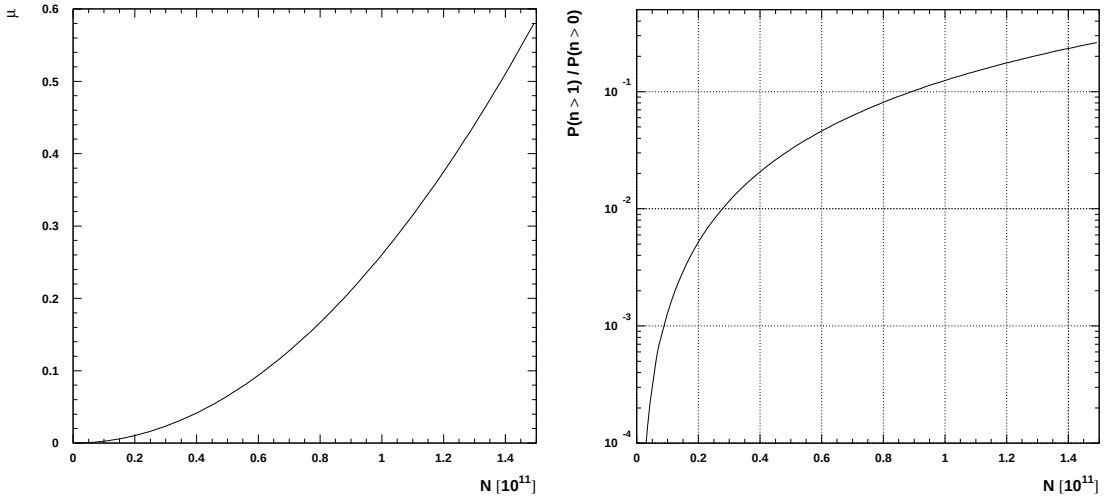

Figure 4: *Pileup as a function of the bunch population at $\beta^* = 90\,m$. Left: mean number of interactions per bunch crossing, μ. Right: conditional pileup probability, $P(n>1)/P(n>0)$.*

3.2 Luminosity reach at $\beta^* = 90\,\mathrm{m}$

The luminosities reached with some typical numbers of colliding bunches, k, and of bunch populations, N, for $\beta^* = 90\,\mathrm{m}$ are listed in Table 4.

As explained in the previous section, before the installation of timing detectors the bunch population should not exceed 0.7×10^{11} protons in order to keep the pileup contamination under control.

With increasing number of colliding bunches three types of fills can be distinguished:

- $k = 1,2$: RP alignment fills with very close distances from the beam centre ($\sim 5\,\sigma$). These conditions are ideal for low-$|t|$ elastic scattering and total cross-section measurements. How-

ever, due to the absence of any collimator hierarchy constraints and loss-map validations, stable beams cannot be declared, thus forbidding the operation of the CMS tracker.

- $2 < k \leq 156$: This is the domain of conventional $\beta^* = 90\,\text{m}$ fills without crossing angle, as implemented before LS1. In such fills the collimation hierarchy constrains the RPs to distances not closer than about $11\,\sigma$ from the beam centre. Data collection is carried out in 'Stable Beams' mode, allowing all CMS subdetectors to be operated. The highest number of colliding bunches injected so far was $k = 108$ in July 2012, while the maximum number compatible with zero crossing angle is 156.

- $k > 156$: To push the number of bunches beyond 156 it is planned to commission a new version of the $\beta^* = 90\,\text{m}$ optics with a crossing angle. In this way bunch spacings as small as 75 ns can be envisaged, allowing for up to 936 bunches [38].

Table 4: *Luminosity [$cm^{-2}s^{-1}$] at $\beta^* = 90\,m$, $\sqrt{s} = 13\,TeV$ and $\varepsilon_N = 2\,\mu m\,rad$, for different numbers of colliding bunches, k, and of bunch populations, N.*

k	N [10^{11} p]			
	0.5	0.7	1.15	1.5
1	8.6×10^{27} (0.74 nb^{-1}/d)	1.7×10^{28} (1.5 nb^{-1}/d)	4.6×10^{28} (4.0 nb^{-1}/d)	7.8×10^{28} (6.7 nb^{-1}/d)
2	1.7×10^{28} (1.5 nb^{-1}/d)	3.4×10^{28} (2.9 nb^{-1}/d)	9.1×10^{28} (7.9 nb^{-1}/d)	1.6×10^{29} (14 nb^{-1}/d)
108	9.3×10^{29} (80 nb^{-1}/d)	1.8×10^{30} (156 nb^{-1}/d)	4.9×10^{30} (423 nb^{-1}/d)	8.4×10^{30} (726 nb^{-1}/d)
156	1.3×10^{30} (112 nb^{-1}/d)	2.6×10^{30} (225 nb^{-1}/d)	7.1×10^{30} (613 nb^{-1}/d)	1.2×10^{31} (1.0 pb^{-1}/d)
468 (150 ns)	4.0×10^{30} (0.33 pb^{-1}/d)	7.9×10^{30} (0.64 pb^{-1}/d)	2.1×10^{31} (1.7 pb^{-1}/d)	3.6×10^{31} (2.9 pb^{-1}/d)
702 (100 ns)	6.0×10^{30} (0.49 pb^{-1}/d)	1.2×10^{31} (0.98 pb^{-1}/d)	3.2×10^{31} (2.6 pb^{-1}/d)	5.4×10^{31} (4.4 pb^{-1}/d)
936 (75 ns)	8.1×10^{30} (0.66 pb^{-1}/d)	1.6×10^{31} (1.3 pb^{-1}/d)	4.3×10^{31} (3.7 pb^{-1}/d)	7.2×10^{31} (6.2 pb^{-1}/d)

For the first year after LS1, a scenario with $k = 936$ and $N = 0.7 \times 10^{11}$ would be ideal. The luminosity of up to $1.6 \times 10^{31}\,\text{cm}^{-2}\text{s}^{-1}$ would enable the collection of $1.3\,\text{pb}^{-1}$ in 24 hours. Assuming a Hübner factor (accounting for machine availability and luminosity decay) of $H = 0.5$, the goal of collecting $10\,\text{pb}^{-1}$ would be reached in 15 days of beam time. However, the planned suppression of the 75 ns bunch spacing option in the LHC injector chain [**?**] would lead to an operation with 100 ns bunch spacing, allowing for at most 702 bunches or a peak luminosity of $0.98\,\text{pb}^{-1}$ per 24 hours. In this scenario, a running time of 15 days at $H = 0.5$ would yield $7\,\text{pb}^{-1}$. To maximise the Hübner factor, a luminosity levelling option via beam separation is currently being explored. After injecting beams with a higher bunch population, a manageable pileup level would be achieved by separating the beams in the IP. During the fill, the luminosity decay would then be counteracted by a stepwise reduction of the beam separation. For example, a bunch population of $N = 1.15 \times 10^{11}$ with an initial separation of $2\,\sigma$ would result in $\mu = 0.13$, the same as for $N = 0.7 \times 10^{11}$ without separation. Note however, that possible adverse effects of this levelling strategy on details of the proton transport by the beam optics have to be carefully evaluated.

At a second stage, after the installation of the timing detectors, the tolerance for a higher bunch population and for the related pileup will improve the statistics by about an order of magnitude.

3.3 Commissioning and start-up strategy

After the recommissioning of the β^*-desqueeze at the new beam energy of 6.5 TeV, the crossing-angle – probably with a size of $\pm 70\,\mu\text{rad}$ – will be introduced.

The RP units to be commissioned at $\beta^* = 90\,\text{m}$ are 220-N, 220-F and the 8^o-rotated 210-F. The first step will be the beam-based alignment with two bunches, followed by a physics run

in the same fill with the RPs very close to the beam, so as to measure low-$|t|$ elastic scattering and the total cross-section with the optical theorem. Afterwards the RPs will be placed in the positions determined by collimation hierarchy for validation by loss maps. This is a prerequisite for operation in stable beams.

After completion of the commissioning, the physics fills can take place. The beam intensity is expected to be gradually raised in the first few fills by increasing the number of bunches with the objective to reach 936 bunches with a spacing of 75 ns or 702 bunches with a spacing of 100 ns.

4 Physics and Detector Performance

This section describes the expected performance of the upgraded detectors in the running conditions requested by TOTEM for its measurements, separately for the tracking and the timing part.

4.1 Tracking detectors

4.1.1 Roman Pots

The Roman Pot (RP) of TOTEM are equipped with 66 μm-pitched high efficiency silicon telescopes which provide spatial resolution of 10 μm (Figure 5). In order to optimise proton acceptance and reconstruction of the scattered protons that arrive at the RPs after traversing a 220 m-long LHC lattice segment, special high-β^* LHC running conditions were designed. The $\beta^* = 90$ m optics [39] has been proven to be the best option for this measurement. The acceptance is further improved with vertical RPs approaching the LHC beams at distances even smaller than 10$\times$beam RMS. The design of the near-beam system is supported by our experiment's practical experience in RP alignment procedures as well as in machine optics evaluation and estimation, which allows to fully profit from the tracking capabilities of the RP devices, as it has been demonstrated with elastic scattering measurements [40, 41]. Remarkably, the $\beta^* = 90$ m optics sensitivity to machine imperfections is relatively small from the viewpoint of data analysis [41].

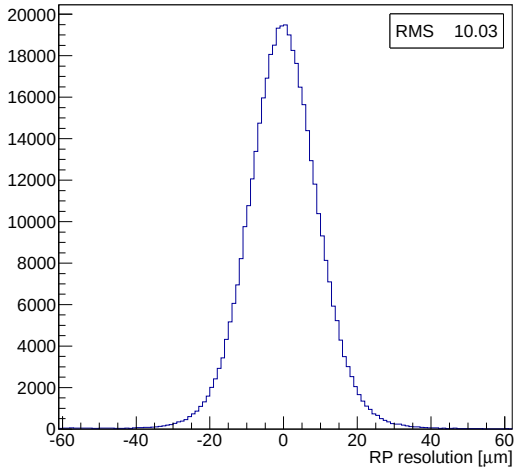

Figure 5: *One arm spatial resolution; average resolution of the RP detectors of a near and far station; data from $\beta^* = 90$ m.*

Intact protons that have lost energy in the primary interaction emerge transversly after passing through the bending magnets. The trajectory of protons produced with transverse position (x^*, y^*) and angle (Θ_x^*, Θ_y^*) at the IP location (the '*' superscript indicates the IP location at IP5) is described by the equation

$$\vec{d} = T \cdot \vec{d}^* , \tag{1}$$

where the vector $\vec{d} = (x, \Theta_x, y, \Theta_y, \xi = \Delta p/p)^T$ and T is the transport matrix; p and Δp denote the nominal beam momentum and the proton longitudinal momentum loss, respectively. The transport

matrix is defined by the optical functions as:

$$T = \begin{pmatrix} v_x & L_x & m_{13} & m_{14} & D_x \\ \frac{dv_x}{ds} & \frac{dL_x}{ds} & m_{23} & m_{24} & \frac{dD_x}{ds} \\ m_{31} & m_{32} & v_y & L_y & D_y \\ m_{41} & m_{42} & \frac{dv_y}{ds} & \frac{dL_y}{ds} & \frac{dD_y}{ds} \\ 0 & 0 & 0 & 0 & 1 \end{pmatrix} \tag{2}$$

where the magnification $v_{x,y} = \sqrt{\beta_{x,y}/\beta^*}\cos\Delta\phi_{x,y}$, and the effective length $L_{x,y} = \sqrt{\beta_{x,y}\beta^*}\sin\Delta\phi_{x,y}$ are functions of the betatron amplitude $\beta_{x,y}$ and the relative phase advance up to the RP location $\Delta\phi_{x,y} = \int_{\mathrm{IP}}^{\mathrm{RP}} \frac{\mathrm{d}s}{\beta(s)_{x,y}}$. Together with the dispersion $D_{x,y}$ (where nominally $D_y = 0$), they are of particular importance for the reconstruction of the proton kinematics. The elements of T depend on proton longitudinal momentum loss ξ.

The $\beta^* = 90\,\mathrm{m}$ optics, which seems the most convenient for soft central diffraction (CD) studies, uses the standard injection optics and the beam conditions typical for the early LHC running with a low number of protons per bunch leading to a pile-up of a few percent.

Proton acceptance The parallel-to-point focusing, which eliminates the dependence on the transverse position of the proton at the collision point, is available vertically ($v_y = 0$). At the same time, a large effective length $L_y = 263\,\mathrm{m}$ at RP location ensures a sizable vertical displacement of scattered protons from the beam centre, which is practically independent from their longitudinal momentum loss $\xi = \Delta p/p$. This leads to about 40 % acceptance of low CD masses for RP positioned at 10σ from the beam center (Figure 6) and allows for detection of the entire ξ-range.

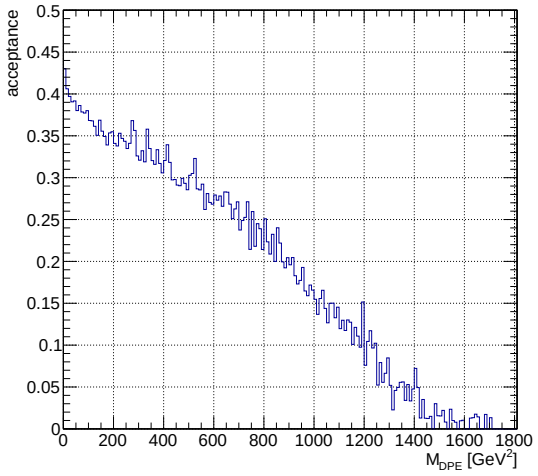

Figure 6: *Acceptance for detecting both protons with $\beta^* = 90$ m optics as a function of the diffractive mass for inclusive central diffractive events (generated with PHOJET [43]). RPs are at 10σ from the beam center.*

Reconstruction resolution The resolution of a vertical scattering angle component is limited only by the beam divergence (2.6 μrad for $\sqrt{s} = 8\,\mathrm{TeV}$, Figure 7 (left)). This can be scaled to a vertical p_T resolution of 12 MeV for the protons for $\sqrt{s} = 13\,\mathrm{TeV}$ and $\varepsilon_N = 2\,\mu\mathrm{rad}$.

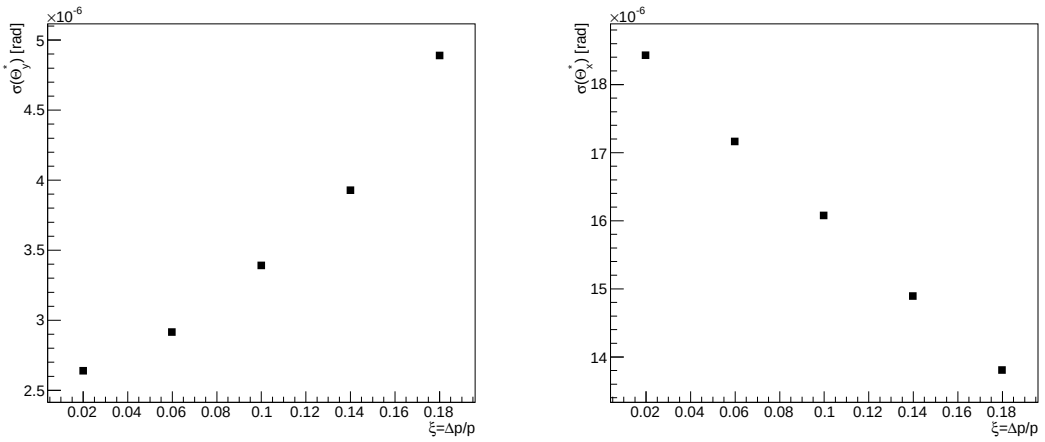

Figure 7: *Angular resolution for detection in the vertical (left) and horizontal (right) plane from a sample of diffractively scattered protons (the first bin contains data points with* $\xi \leq 0.02$*).*

Since the horizontal displacement of protons x is both caused by the scattering angle Θ_x^* (via L_x which is close to 0) and ξ (via D_x), the reconstruction of both variables is correlated (correlation factor of 89 %). The resolution of Θ_x^* obtained for $\sqrt{s} = 8\,\text{TeV}$ runs was $20\,\mu\text{rad}$, as can be seen in Figure 7 (right). This can be extrapolated to a horizontal p_T resolution of 91 MeV for the protons for 6.5 TeV beams and normalised emittance $\varepsilon_N = 2\,\mu\text{rad}$.

Transverse position measurement allows also for precise proton azimuth angle determination with $\sigma(\phi)$ resolution typically in the range of $9 \times 10^{-2} - 4 \times 10^{-1}\,\text{rad}$, depending on the four-momentum transfer t [42]. One of the components of the spin analysis of the observed resonances will be the azimuth angle difference $\Delta\phi_{1,2}$ study within the pairs of protons.

The large interaction point size ($113\,\mu\text{m}$ with this optics) will limit the absolute ξ-resolution to 0.6 %. This means that very low-ξ protons can be tagged with high acceptance by the RPs even when their forward momentum loss ξ cannot be reconstructed.

Vertex reconstruction As it has already been mentioned, for low-ξ protons, L_x at the RP locations is close to 0. This allows to eliminate the horizontal scattering angle from Equation 1 and solve it for x^* (the interaction vertex):

$$x^* = \frac{x_{RP} - \xi D_x}{v_x}, \tag{3}$$

which opens a possibility of reconstruction of the horizontal vertex position component for each of the two protons. The comparison of two reconstructed values will provide a cut against the pile-up, effective for $\xi \lesssim 0.1\%$. The low-ξ limit is determined by the optimal x^* reconstruction resolution of $5.9\,\mu\text{m}$ and the optical functions. Although such a pile-up rejection will not be effective for the complete ξ-range, it will be applicable to diffractive masses below 10 GeV for $\sqrt{s} = 13\,\text{TeV}$, which is the region of major interest for 2015 runs.

4.1.2 CMS Tracker

The CMS Tracker is a versatile detector of excellent tracking capabilities designed for efficient and precise reconstruction of the trajectories of charged particles with transverse momentum above 1 GeV in the pseudorapidity range of $|\eta| < 2.5$ [44, 45].

Among the most important physics cases is the exclusive central diffractive production of low mass resonances ($M_X <$ a few GeV) ultimately decaying into charged hadrons. In particular, mass distributions of $\pi^{+/-}$ and $K^{+/-}$ neutral configurations are of high interest. Detailed measurements of cross-sections and branching ratios at $\sqrt{s} = 13\,\text{TeV}$ will provide important insight into diffractive resonance production as well as may shed light on current understanding of glueball candidates present in this range, provided sufficient luminosity is integrated.

Acceptance and resolution Special tracking algorithms, for instance as presented in Reference [46], extend the tracking capabilites down to $p_T \approx 0.1\,\text{GeV}/c$, as can be seen in Figure 8.

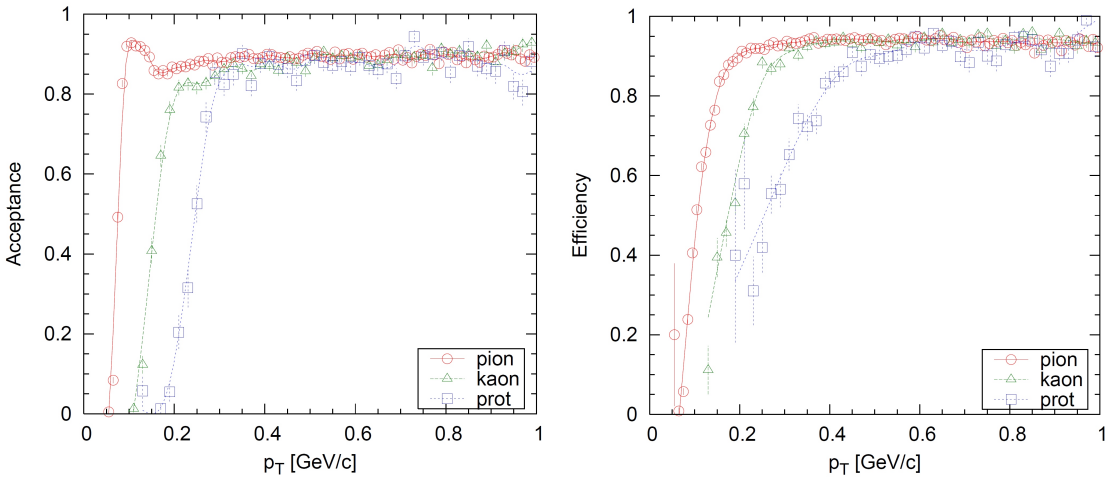

Figure 8: *CMS Tracker acceptance (left) and reconstruction efficiency (right) as a function of p_T, for tracks in the range $|\eta| < 1$, for pions (circles), kaons (triangles) and protons (squares). Published in [46].*

They have been successfully applied to studies requiring low p_T tracks reconstruction. In particular they yielded excellent results in analyses of low mass spectra acquired both with pp and pPb collisions [47, 48]. An absolute p_T resolution of about $0.02\,\text{GeV}/c$ in the p_T range of 0.1 – $2\,\text{GeV}/c$ [47] can be provided, which is of high interest for the physics program presented in Chapters 1 and 2.

The good p_T resolution of the Tracker allows for precise diffractive mass determination with $\sigma(M_X) \approx 20 - 30\,\text{MeV}/c^2$, which is significantly smaller than the reported widths of 0^{++} and 2^{++} resonances, typically of $\sim 100 - 200\,\text{MeV}$, present in the mass range of $0.5 \lesssim M_X \lesssim 4\,\text{GeV}$.

For completely reconstructed CD events with final states composed of charged tracks only, a combined CMS-TOTEM kinematics reconstruction can be conceived. It should theoretically allow for ξ_1 and ξ_2 reconstruction with a precision of the beam momentum spread (10^{-4}) together with improved, by a factor of 2, RP horizontal p_T resolution. Such combined CMS-TOTEM kinematics reconstruction will be studied in detail in the near future, when a common software release will be available.

Particle identification (PID) Tracker-based PID is based on the relationship between energy loss rate and total momentum [47]. Standard CMS PID makes use of strip detectors limiting p_T to above $\sim 0.5\,\text{GeV}$. However, the physics programme discussed in the present document, requires preferably PID availability in the complete p_T range for which momentum reconstruction is possible. Therefore, it is necessary to use both strip and pixel silicon devices together with appropriate

calibrations. PID capabilities extend down to $p_T \approx 0.1\,\mathrm{GeV}/c$ [47]. Due to the overlaps of energy loss rate curves for higher momenta, as it is illustrated by Figure 9, PID capabilities are nevertheless restricted to $p < 0.15\,\mathrm{GeV}/c$ for electrons, $p < 1.20\,\mathrm{GeV}/c$ for pions, $p < 1.50\,\mathrm{GeV}/c$ for kaons, and $p < 1.70\,\mathrm{GeV}/c$ for protons. Despite momentum limitations, the available PID range is sufficient to discriminate between branching ratios leading to pairs of $\pi^{+/-}$ or $\mathrm{K}^{+/-}$ in the mass range of 1 – 2 GeV. However, in case of χ_c only the topologies of 2 or 3 $\pi^+\pi^-$ pairs are potentially identifiable.

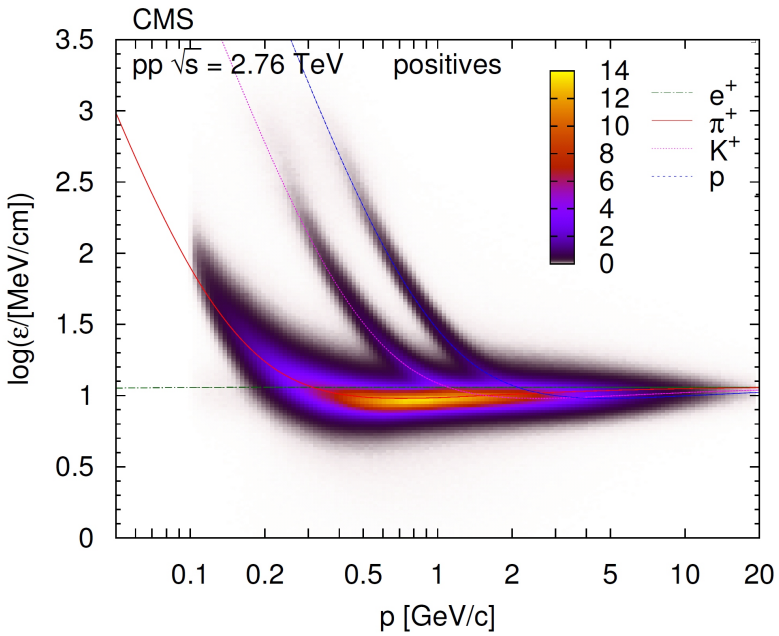

Figure 9: *CMS Tracker distribution of the logartithm of most probable energy loss rate* ε *[49] as a function of total momentum p for the CMS* 2.76 *TeV dataset, for positive particles. The z scale is shown in arbitrary units and is linear. The curves show the expected* $\log(\varepsilon)$ *for electrons, pions, kaons, and protons [47].*

Finally, the CMS Tracker provides vertex position information. Unfortunately, compared to hard processes, for soft interactions such as CD, involving merely a few low-p_T tracks, CMS vertex reconstruction is limited. Available transverse vertex position precision is of the order a few hundred microns (compared to the interaction size of $113\,\mu$m for $\beta^* = 90\,$m runs). On the contrary, longitudinal vertex reconstruction, with precision of a few milimeters (corresponding to a few ps), will be of high importance in discriminating between overlapping events when combined with the TOTEM timing detectors.

4.1.3 Combined CMS and TOTEM detectors

Combined, the CMS and TOTEM detectors provide comprehensive description of the interaction. The Tracker measures precisely the diffractive mass M_X and p_T of the final state. It provides precise information about track topologies and their momenta, which is a valuable input for final state spin analysis and for the decay chain reconstruction. RP detectors determine angular correlations within proton pairs providing insight into angular momentum configurations of particles exchanged within the interaction together with the p_T of each of them.

CD signal selection strategy The combined detectors bring significant tagging enhancements, which provide effective means of pile-up reduction for CD processes. The selection strategy is based on the following available cuts:

1. Despite limited ξ-resolution, RP detectors provide efficient ξ-independent trigger of 2 arm coincidences. In this way CD events' selection does not need to rely on rapidity gaps, which are subject to statistical fluctuations, but directly on tagged protons.

2. Charged particle tracks reconstructed in the Tracker are a signature of an inelastic process.

3. Requested specific numbers of charged tracks in the Tracker corresponding to the event topology of interest. E.g. pairs of charged particles may be requested.

4. TOTEM timing detectors installed in vertical RP devices will assure that protons reconstructed in 2 arms originate from the same interaction vertex suppressing in this manner the pile-up induced by beam halo and diffractive processes. Furthermore, longitudinal CMS vertex reconstruction [50, 51] of a few-milimiter-precision should be obtainable for low multiplicity soft events. This can be combined with the TOTEM timing detectors further assuring that CMS Tracker and RP detectors reconstruct the same event (in particular further reducing elastic pile-up). This capability is of key importance for studies of low cross-sections (in the range of pb) with beam conditions of average number of inelastic pp interactions per bunch crossing $\mu = 50\,\%$.

5. The p_T of the diffractive system reconstructed by CMS should be exactly opposite to the transverse momentum reconstructed by the RP devices (especially the vertical component can be effectively employed due to more comparable resolution). Such a cut of a width of $\sim 50\,\mathrm{MeV}$ will efficiently reduce pile-up and assure exclusivity.

6. CD mass system (assuming all its particles are detected) has to be charge neutral, which can be assured by the Tracker. On the contrary, a request of charge imbalance will provide a tool for background estimation.

7. For low-ξ protons, corresponding approximately to masses below $10\,\mathrm{GeV}$, RP detectors can reconstruct horizontal component of the interaction vertex for each arm independently. Comparison of these two values will provide an effective tool for pile-up rejection.

8. T2 in veto in both arms enforces rapidity gaps, effectively suppressing SD pile-up.

9. Different charged particle branching topologies can be discriminated by performant PID within the p_T and η range of interest.

Pile-up rejection for low CD masses (2015 runs) According to the physics programme detailed in Section 2 and Table 1, CD triggered by a pair of protons with $0.5 < M_X < 4\,\mathrm{GeV}$ is the target signal. For $\beta^* = 90\,\mathrm{m}$ and $\mu = 5\,\%$ runs with the RPs placed at 10σ from the beam center, the key pile-up contributions for low masses are the following:

- **Minimum bias events.** From current LHC measurements (e.g. [52]) it can be extrapolated that for $\sqrt{s} = 13\,\mathrm{TeV}$ $\mathrm{d}N/\mathrm{d}\eta_{\mathrm{ch}} \approx 7.7$. Assuming Poisson distribution and $|\eta| < 2.4$ range, the probability of having exactly 2 or 4 charged tracks (Cut 3) is respectively 5×10^{-14} and 6×10^{-12}. Applying further Cut 6, the probabilities are reduced to approximately 3.8×10^{-14} and 4.1×10^{-12}, respectively. In coincidence with elastic scattering (detected cross-section $\approx 10\,\mathrm{mb}$), $\mu = 5\,\%$ and integrated luminosity $L = 10\,\mathrm{pb}^{-1}$, it yields less that one event in total.

- **CD**. About 60–75% of CD events will not have a proton signature due to the acceptance in-t. However, in coincidence with elastic scattering, they can create a fake signature with protons detected in RPs not corresponding to the diffractive mass M_X. In the 2015 runs we are interested mainly in the mass range of $0.5 < M_X < 4\,\text{GeV}$. The effective CD cross-section where neither of the two protons are detected in the RPs in this mass range is about 0.15 mb (out of 1 mb of assumed CD cross-section). This fake signal can be suppressed by Cut 5. The $p_{y,\text{CMS}}$ distribution can be approximated by Gaussian density with $\sigma = 0.5\,\text{GeV}$. With a p_y cut of 50 MeV width the fake signal is reduced by a factor of 9. Within the low mass range, about 30 % and 6 % of reconstructed CD events contain 2 or 4 detected charged tracks.

  For $\mu = 5\,\%$, $L = 10\,\text{pb}^{-1}$ and $0.5 < M_X < 4\,\text{GeV}$, average numbers of 2300 events / 100 MeV ($N_{ch} = 2$) and 450 events / 100 MeV ($N_{ch} = 4$) are obtained in the studied range.

- **SD.** About a half of ~ 14 mb of assumed SD cross-section will be characterised by the proton not detected due to its t-distribution. Similarly to CD, SD has to occur in coincidence with another process (or processes), which can provide a pair of protons to be tagged by the RPs. Elastic scattering, for its high cross-section, again would the most probable candidate. However, SD produces relatively high and forward diffractive systems. This is characterised by the correlation between the central mass $M_{X,\text{SD}}$, the forward proton momentum loss ξ and the rapidity gap $\Delta\eta$ (between the leading proton, in this case not detected, and the diffrative system): $M_{X,\text{SD}} \approx \sqrt{s \cdot \xi} \approx \sqrt{s} e^{\frac{-|\Delta\eta|}{2}}$. For $\sqrt{s} = 13\,\text{TeV}$ and $M_{X,\text{SD}} \lesssim 4\,\text{GeV}$, $\xi \lesssim 10^{-7}$ and $\Delta\eta \gtrsim 16$. Such a rapidity gap completely comprises the Tracker, highly suppressing any pile-up in coincidence with SD.

- **Beam halo** induced pile-up will be at least an order of magnitude less harmful than the elastic scattering. It requires two concident beam halo protons together with a CD event (or some equivalent combination), which already reduces its probability. In addition Cut 7 is applicable.

The expected pile-up should not pose a problem for the running scenarios proposed for 2015 (Table 1). Despite the uncertainties of the MC generators, such background can be well parameterised from the physics data. However, it limits the experimental sensitivity. A 5-σ significance claim would require at least $\sim$240 events ($N_{ch} = 2$) and $\sim$110 events ($N_{ch} = 4$), assuming a typical 100 MeV width and $\mu = 5\,\%$. For integrated luminosity $L = 10\,\text{pb}^{-1}$ it corresponds to sensitivity to cross-sections of $\sigma > 240\,\text{pb}$ and $\sigma > 110\,\text{pb}$, respectively (combined CMS-TOTEM acceptance of 10 % included). Timing detectors per arm of about 50 ps resolution would increase the sensitivity by a factor of 2–3. For runs with $\mu = 10\,\%$ and integrated luminosity $L = 10\,\text{pb}^{-1}$, the sensitivity to cross-sections would lower by about a factor of $\sqrt{2}$, and they would be $\sigma > 340\,\text{pb}$ and $\sigma > 160\,\text{pb}$, respectively.

Pile-up rejection hard CD di-jets (2016 runs) In this case hard diffractive processes are of concern (mainly hard CD) and higher masses (typically hundreds of GeV/c^2), together with higher proton forward momentum losses, are involved. The event description can profit now from RP ξ-reconstruction. The di-jet trigger will be a baseline of event tagging.

The pile-up break down is dominated by a QCD di-jet[1], in coincidence with a soft diffractive process[2], mimicking a hard CD event. Among the pile-up contibutions (soft CD $\times$ QCD di-jet, hard SD $\times$ soft SD, soft SD[2] $\times$ QCD di-jet, hard DPE $\times$ SD) a coincidence of a QCD di-jet together with a soft CD is dominating [32]. The other contributions in total account for less than the leading one.

[1] simulated with PYTHIA [53]

[2] simulated with PYTHIA [53] and PHOJET [43]

For running conditions assuming $\mu = 50\,\%$ and $\beta^* = 90\,\mathrm{m}$, probability per bunch crossing of a QCD di-jet ($p_T > 15\,\mathrm{GeV}/c$) appearing together with a soft CD (within combined CMS-TOTEM acceptance) is 1.4×10^{-6}. TOTEM timing detectors of about 50 ps, in conjunction with CMS vertex reconstruction (Cut 4), will reduce this probability significantly by about a factor of 5–10. As it was observed in the pilot CMS-TOTEM runs in 2012, kinematics cuts requiring four-momentum conservation can further reduce such pile-up by a factor of 5. Furthermore, in case of exclusive searches (e.g. exclusive di-jets within $|\eta| < 5$), T2 in veto in both arms (Cut 8) will reduce the CD component by a factor of about 15, as it was observed from TOTEM standalone 2012 data. Cut 8 will also effectively suppress the QCD inclusive di-jet contamination removing about 90–95 % of it. One more possibility of pile-up reduction is offered by the approach discussed in [55], applied by ATLAS, which consists in a cut on the additional tracks at the vertex.

In total, including all pile-up sources, a number of 12 k fake events can be expected for $L = 100\,\mathrm{pb}^{-1}$, which allows for a sensitivity of 5 pb at 5σ significance.

Signal selection strategy will be further studied and improved with soon-to-be-available common CMS-TOTEM software release.

4.2 Timing detectors

Due to the machine background and the pileup more than one track per bunch crossing can arrive to the RP. The electronics associated to the timing detector (see section 5.1.2) can measure without ambiguity only the traversing time of one particle per bunch crossing, hence the detector plane must be properly segmented. The signal and background rates are discussed in the next section and, in the following one, the way the timing information may be used to improve the trigger selection for the high luminosity runs.

4.2.1 Optimization for physics signal and background rates

A Monte Carlo (MC) simulation, tuned by the cross section values listed in Table 5, is used to estimate the primary proton yields. The values refer to 7 TeV measurements already published by TOTEM [3, 4, 6].

Table 5: *Cross section values used in the simulation.*

σ_{TOT}	98 mb [3]
σ_{EL}	25.1 mb [4]
$\sigma_{INEL-VISIBLE}$	70.3 mb [6]
$\sigma_{INEL-INVISIBLE}$	2.6 mb [6]
σ_{SD}, 3.4<M<7 GeV	1.8 mb
TimingDetectors.tex σ_{SD}, 7<M<350 GeV	3.3 mb
σ_{SD}, 0.35<M<1.1 TeV	1.4 mb
σ_{SD}, M>1.1 TeV	1 mb
σ_{CD}	1 mb

Considering that the average number of interactions per bunch crossing is determined by the

pile-up probability, only ratios of the different cross sections are relevant. In this work it is assumed that these ratios will not change much when the center of mass energy varies from 7 to 14 TeV.

The inelastic cross section values are given for selection of events with particles seen only in one arm of T2 (26%) and events with tracks in both T2 sides (74%). Diffractive events with masses M<1.1 TeV are inelastic events with activity in only one arm of the T2 telescope, while for larger diffractive masses the events must see tracks in both T2 telescopes. The elastic scattering is simulated with an exponential t-distribution, as measured by TOTEM [1].

The beam induced background plays an important role in determining the final rate to be discriminated with the timing detectors [56]. Background sources in this study are classified in two main categories: the "collision debris" and the "beam halo".

The first contains non-leading protons transported from the IP to the RP or particles from showers in vacuum pipe aperture limitations that eventually generate a signal in the RPs. This fraction of the background is expected to scale with the number of vertices generated in the bunch crossing.

The second contribution is due to beam protons traveling far from the central beam orbit that hit the RPs; this contribution is expected to scale with the beam current[3]. In this study the background is calculated per bunch crossing and the effective scaling is done based on the parameter μ, defined as the mean number of inelastic interaction per bunch crossing. Hereafter all particles arriving at the RP which are not leading protons will be considered as background.

The expected background in the new running conditions is estimated using a sample of recorded data in well defined conditions ($\beta^* = 90$ m, $\sqrt{s} = 8$ TeV and μ =0.05, with the vertical RPs inserted at $9.5\,\sigma$ from the beam). The background rates in a "Zero Bias" (random trigger on bunch crossing) triggered sample are extrapolated to higher pile-up conditions. More details on the background extrapolation are reported in [56].

The beam halo contribution was calculated for Zero bias events as the probability to have a proton track reconstructed in the vertical RPs when both T2 arms are empty and no elastic signature is present (ie no collinear protons on the other arm). The estimate is conservative and probably overestimates the beam-halo, as the selection includes contributions from low mass SD (no signal in T2 with possibly a single proton in the RPs acceptance) and a small fraction of elastic events with a proton on one arm escaping the detection (due to smearing and edge effects). This background, assumed to scale with $\sqrt{\mu}$, is $\approx 2-3\%$ for each vertical RP in condition with μ =0.5-1.

The beam-beam background has been estimated by selecting events with tracks in both arms of T2: in this subsample the probability to have at least a cluster in the RPs for events without elastic candidates was found to be 1.5%. In this estimate the contribution of the high-mass diffraction is already subtracted (about 0.5%).

In conclusion, the background probability estimated for a scenario with high-β^* and μ =0.5 is about 3% per BX, including beam-halo and beam-beam effects. The measured RP track multiplicities have then to be corrected to account for the limited (multi)track reconstruction capability of the RP detectors during the LHC RUN1, especially in events containing a shower. A more precise estimate of the multiplicity at high pile-up is obtained using the number of clusters defined as a group of neighboring strips with signal in one plane of the RP detector. Hereafter we define the "cluster multiplicity" as the average number of clusters in the 10 planes of a RP detector package. Plots in figure 10 shows the inclusive cluster multiplicity as obtained from the simulation (right) and as measured from the data (left) for a $\mu = 0.05$, i.e. in a condition in which the pile-up fraction is minimal. The multiplicity of a sector presented in the plot is the sum of the top and bottom RP multiplicities.

[3] In fact $I_{beam} \propto n_{bunch} N_{proton}$, where n_{bunch} is the number of bunches in the LHC ring and N_{proton} is the number of protons in a bunch, while the pile-up is proportional to N^2_{proton}.

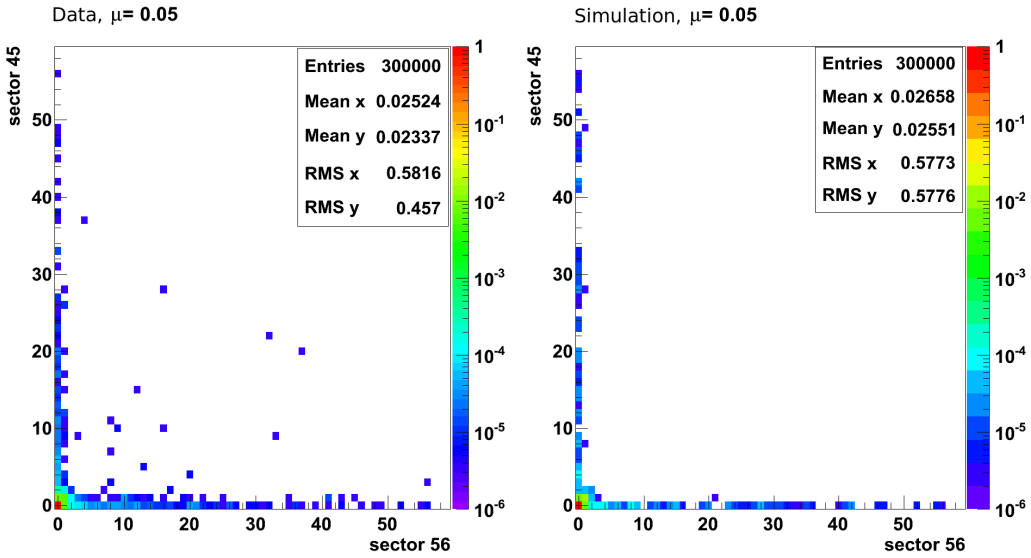

Figure 10: *Cluster multiplicity for μ = 0.05 measured in the vertical RPs: data (left) and simulation (right).*

The beam halo background is included in the simulation by taking into account the position of the halo tracks and the left-right multiplicity correlation. Figure 11 shows the inclusive cluster multiplicity for runs at a higher value of μ =0.5, calculated by extrapolating the yield of primary and background tracks as previously described.

Finally values for the occupancy are shown in Figure 12 for $\mu = 0.5$. The occupancy values reported in Figure 12 are not corrected by a factor 1.2 to account for the limited multi-track capability.

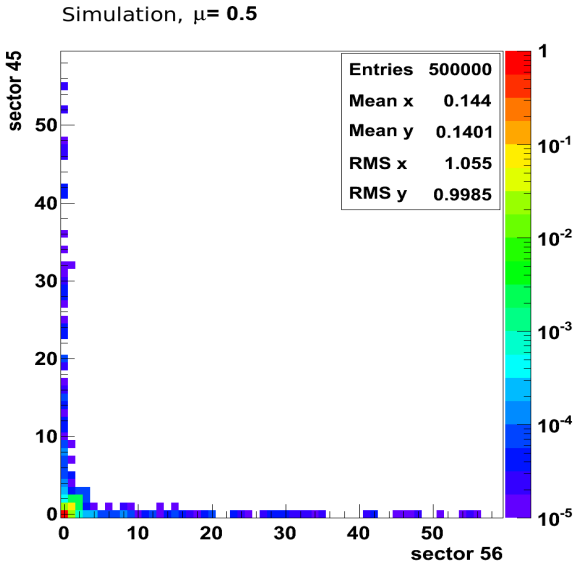

Figure 11: *Simulated track multiplicity (signal + background) per bunch crossing in the vertical RPs, in the case of μ = 0.5.*

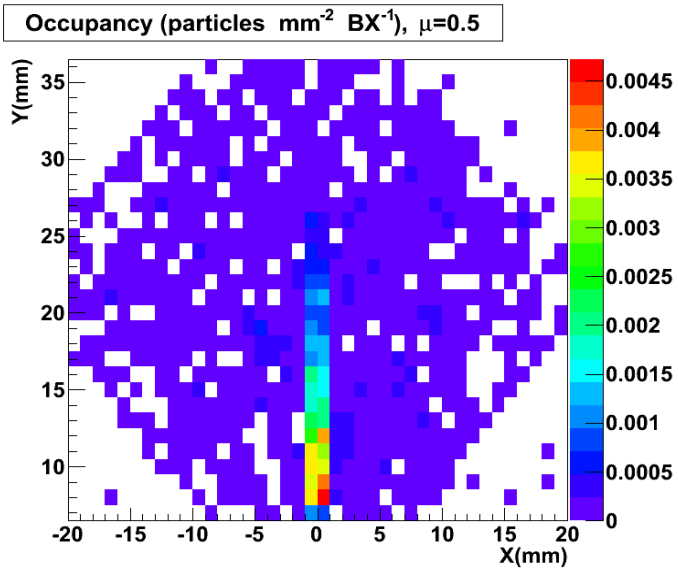

Figure 12: *Occupancy/BX in the vertical RP ($\beta^* = 90$ m, $\sqrt{s} = 8$ TeV and $\mu = 0.5$). A correction factor of 1.2 to account for multiple tracks inefficiency is not included in the plot (see text).*

The last step of this study is to define the best configuration of the timing detector segmentation trying to keep the number of channels low and yet maintain the proper efficiency for timing measurements, since limitations of the readout electronics due to the rise time of the signal amplifiers do not allow to discriminate between two hits in the same cell.

The optimized readout geometry of the timing detector (see Figure 13) takes into account both the geometry constraints and the double hit probability such that each cell has a constant loss due to double hit. For the final determination of the geometry the signal due to the elastic interactions, which is the dominant source of the detector occupancy, has been taken into account.

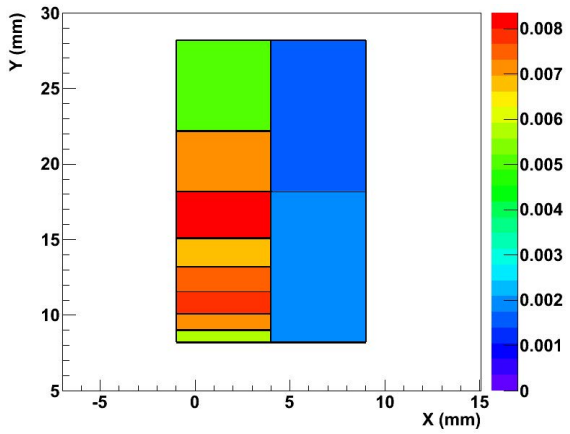

Figure 13: *Optimised read-out geometry and the cell occupancy per BX from the simulation of the top-vertical RP.*

The surface is covered by 10 pixels of different sizes: the left column has 8 smaller pixels with an x dimension ranging from 0.8 mm to 6 mm to cope with a larger expected occupancy (see Figure 12). The color code gives the occupancy in each cell.

Figure 14 shows the position of the timing detector when aligned to the tracking detectors from the other RP for a high beta run. In the same figure one sees from a simulation the density of hits in the RP system.

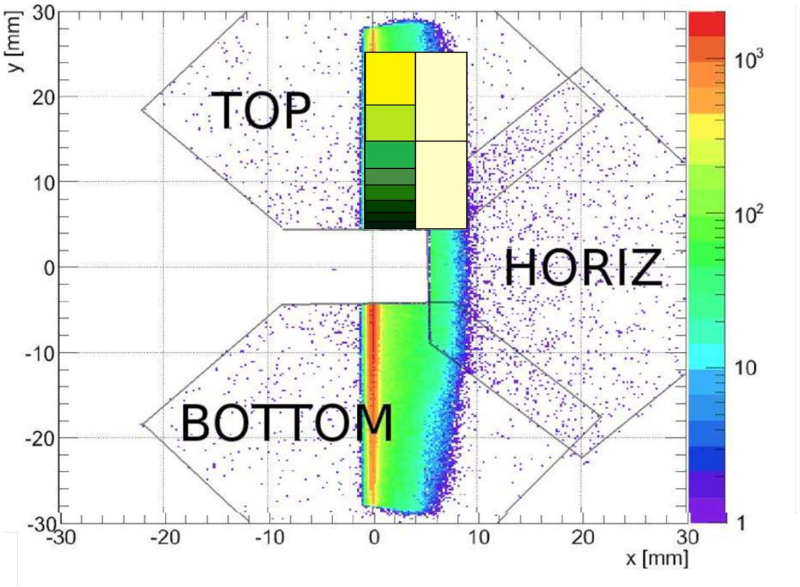

Figure 14: *Tracking and timing detectors aligned during a high beta physics run (from simulation).*

The estimated inefficiency of the DPE event reconstruction due to double hits in the vertical timing detectors is 0.6% at μ =0.5 and 3% at μ =1, which is considered an extreme pile-up condition for the β^*=90 m optics. The study has been repeated to check inefficiencies for more than 2 tracks in the detector imposing a multiplicity cut for events with more than 2 trigger "roads" in the vertical RPs in both arms. The occupancy in this scenario is very low and this extra requirement doesn't significantly affect the efficiency.

4.2.2 Trigger strategy

This section studies the trigger strategy to select the DPE events with optimised efficiency and purity, by using a common CMS/TOTEM trigger algorithm that will include timing detector signals flagging at least one DPE vertex from the measurement of the time of flight of the protons. It is moreover possible, in case the DAQ chain is fully integrated in CMS, to include the timing information from the RP in the High Level Trigger stage (HLT) event selection, the trigger road multiplicity information from the tracking RPs and the vertex-Z position from the Timing RP will be added to the CMS L1 algorithm.

The probability of generating a single (double) arm trigger from the tracking RP detector have been estimated with a simulation. Hereafter "single arm trigger" refers to topologies where only one arm of the RPs has some road trigger reconstructed while in a "double arm" trigger both the sectors 45 and 56 have at least a trigger road. Simulation estimates were performed for different values of μ and give 1.4% (0.9% double arm) for $\mu = 0.05$ and 12% (9%) for $\mu = 0.5$ (more details can be extracted from Table 6). The reported percentages for the single arm trigger configuration refer to the sum of the single arm probabilities of the two configurations: (sector 45 ON and sector 56 OFF) plus (sector 45 OFF and sector 56 ON).

The absolute time at which protons arrive at the RP is the sum of the generated vertex time, the traveling time to the detector (t_d) and an additional uncertainty due to the detector resolution. Background particles attributed from secondary interactions will show a small additional delay due the time spent by the particles to travel an extra-path length before hitting the material of the vacuum chamber at aperture limitations in the LHC lattice. This extra-path length, hereafter assumed of only ~ 3 cm, will be directly measured on data. Tracks detected in opposite arms are paired and for each the relevant observables are the sum and the difference of the arrival times. The

sum, $\bar{t} = \frac{t_1+t_2}{2} - t_d$, provides a check of the proton collision time (bunch) while the difference in the arrival time (Δt) is proportional to the longitudinal position of the collision vertex ($z_{pp} = \frac{c\Delta t}{2}$).

Table 6: *Single and double arm trigger probability from silicon RP detectors.*

	$\mu = 0.05$	$\mu = 0.5$
single arm probab.	0.014	0.12
single arm rate/bunch (kHz)	0.15	1.35
double arm probab.	0.009	0.09
double arm probab. rate/bunch (kHz)	0.1	1

To avoid a large number of combinations for events with a shower developing just in front of the RP, the study is limited to events in which the number of trigger roads[4] reconstructed on each side is not greater than 2. The efficiency of this cut (N-Cut) is still larger than 99%. Having reduced the multiplicity to 2×2, the trigger can compute the four combinations of sum and difference of the arrival times in one clock cycle.

The resolution of the timing detectors is expected to be 50 ps ($\sigma(z_{pp}) \approx 10.6$ mm), to be compared with the rms of the vertex Z-position of $RMS_{bunch}/\sqrt{2} = 7.1$ cm for a rms bunch length of 10 cm.

When TOTEM is running standalone, much of the rate coming from the loose cuts at L1 will be reduced in the offline stage when the datasets of both experiments will be combined. On the contrary if the Totem DAQ is fully integrated in CMS we can profit from HLT trigger. In this case the next step is the matching of the position of vertices from the timing with the list of the primary vertices ($z_{central}$ position) established by the CMS tracker. Due to the effect of the N-Cut a maximum number of 4 candidate vertices can be provided by the timing detectors. Therefore we search in the list of the vertices provided at the CMS-HLT[5] for a match with the ≤ 4 vertices measured by the timing detectors. The event is triggered only if a RP timing vertex is closer than 30 mm to one of the CMS tracker vertices. This cut has an efficiency of about 98%.

The analysis of simulated events for DPE measurement has shown that the main background is due to events where the DPE signature is faked by two opposite protons with at least one of them in the category beam halo background, single diffractive or elastic events. A sample of 500K bunch crossing events has been analyzed and the purity and selection efficiency on the DPE events have been detemined with two experimental configurations, where the RPs are equipped with timing detectors (NEW configuration) or without their addition (OLD configuration) as in the past runs. The results are based on simulations with $\mu = 0.5$ and a rms bunch length of 10 cm.

Only DPE events having both protons in the top RPs or bottom RPs are considered in these analyses as a strategy to remove the elastic protons. The pileup background suppression power of the timing detectors is the same in a configuration in which top-bottom and bottom-top protons are considered, but in this case the rate of the elastic process is summed to the inelastic one. Offline, the presence of inelastic tracks in the central CMS tracker pointing to the protons timing vertex will remove completely the elastic events.

A cut on the "trigger road" multiplicity of the tracking detectors is applied by asking no more than two trigger roads per side of the interaction point.

[4]Each RP detector plane is divided in 16 group of 32 strips. A "trigger road" is defined as at least 3 (out of 5) aligned groups present in a detectors stack.

[5]The CMS vertex reconstruction efficiency is assumed to be 1 for all the interactions reported in tab. 5 except for the elastic and for the SD interactions at M<350 GeV where the efficiency is instead 0.

For $\mu = 0.5$ the trigger probability per bunch crossing (BX) once the N-Cut is applied is expected to be 7%. With the additional requirement that the difference in the distance of the reconstructed vertex between a CMS and the timing ones be less than 3 cm, the rate decreases to 0.2%.

The analysis based on the OLD detector configuration requires a very stringent event selection condition on the maximum number of vertices reconstructed by CMS, i.e. no more than 1 vertex has to be reconstructed by CMS for an unambiguous CMS/TOTEM event matching. Moreover, in this configuration events with more than one reconstructed track per RP cannot be properly analysed, given the inability to properly associate them to the vertex associated to the DPE process.

In the NEW configuration such strict conditions are not needed and assuming an analysis cut on the DZ matching of the CMS-TOTEM vertices of 1cm, we found that the fraction of fake DPE is reduced by about 60% with respect to the OLD configuration, still keeping a similar efficiency (which is of the order of 60% for DPE having both protons in the RP acceptance). The purity can be further increased with the use of a more strict cut on the DZ matching of the CMS-TOTEM vertices, but at the expense of the selection efficiency. Despite the fact that background reduction is here reported for a non diagonal configuration, similar performances are also expected for the diagonal configuration. In this case the elastics protons have to be removed with cuts on the tracking variables as the cms vertex will not be available.

5 Timing Detector System

5.1 Timing detectors

The physics program defines the main specifications for the timing detector to be installed in the vertical Roman Pot.

- Time resolution of ~ 50 ps;
- Low occupancy to reduce inefficiency due to double hit in the same detector;
- High efficiency up to the edge close to the beam to match the acceptance of the existing tracking detectors.

However many other practical considerations had to be taken into account to arrive to a design that could be implemented and properly function in the high radiation environment of the LHC tunnel. In what follows we explain the process that led us to make the choice of the detector that will be installed in the TOTEM RP in LSS5.

5.1.1 Detector segmentation

Extracting timing informations from the Vertical RP system can only be done by installing timing detectors in the existing RP enclosures, where only short longitudinal-sized detector packages can be fitted (up to 5 cm). Cerenkov detectors have been proposed [57] however the dimension required by their radiator is such that they cannot be fitted in the existing vertical RP.

To keep a low occupancy for each detector channel its segmentation must be properly tuned. A simple increase of the granularity reducing the pixel size would lead to an impractical growth of the number of channels, which in turn would reflect on the readout, requiring for example the development of custom ASICs.

This considerations led to study a design with pixel of different sizes since track density due to diffractive and overlapping background is not uniform as can be seen in the RP data recorded during Run-I (see Figure 14). The pixels size is defined in order to have the same track occupancy in all pixels. The simulations to study the occupancy of a single pixel and the minimization of the number of channels required in each detector plane suggested that the minimal number of pixels of different sizes needed for a good efficiency at higher luminosity is 10 per plane with area ranging from few mm^2, for the pixels where the track density is larger, to several hundreds of mm^2 on the external part of the detection plane. The simulation is explained in detail in Section 4.2.

The selection of the detector technology has to take into account the required timing resolution and the variable size of the pixels. The best choice is a diamond sensor, where the pixel size minimally affects the time response of the signal due to the extremely high impedance of the material, guaranteeing the same resolution all over the detector plane. However the charge released from a diamond sensor is small in absolute terms ($\approx$ 15,000 e for a thickness of 500 μm, or ≈ 3 fC/MIP), and a low noise amplifier is needed to keep the S/N ratio large enough. Since the diamond resistivity is very high the main noise source is the first stage of the amplifier. It is also easy to implement a pattern with pixels of different sizes by means of a simple metalization on the diamond crystal. The front end electronics design will be then a compromise between speed and low noise.

The number of channels required is 10 per plane and the preamplifier stage has to be located near the detector itself. A single plane is a 10x20 mm diamond sensor A board built with controlled impedance material (Roger) will be the mechanical support for the detectors, glued with the smallest pixel sizes located near the edge closer to the beam, and for the preamplifier electronics in order to reduce to the minimum the input capacitance (see Figure 15). A package of 4 detector

planes, with thickness up to 500 μm, will fit in a Vertical RP. Among the commercially available diamond substrates it is possible to choose detectors with resolution of the order of 100-150 ps, as the multiple measurements allow to reduce the overall time resolution down to the required $\sim$ 50 ps. The readout board will be located as close as possible to the detector .

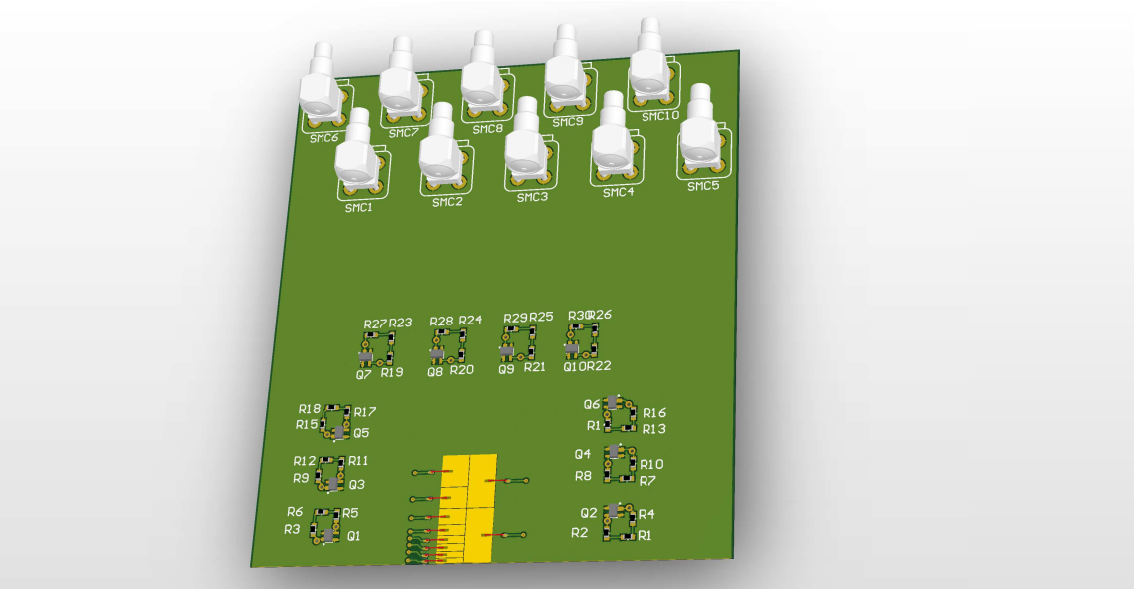

Figure 15: *The layout of the board showing the pixel position for one diamond detector plane.*

5.1.2 Readout electronics

Given the small number of electronics channels required for the readout TOTEM is developing a discrete component amplifiers. This single channel preamplifier is made up of two stages, i) the first is a simple CE transimpedance amplifier, with low amplification power and high bandwidth that allows fine tuning of the input impedance (Silicon-Germanium transistors from Infineon are under test). The controlled output signal has 50 ohms impedance. ii) The next stage amplifies the signal to an output voltage range of 0-1 Volts to match the readout requirements. The detector hybrid will contain only the first stage of the amplification chain and the signals are sent through coaxial cables to the second stage amplification board. The Hybrid is in the secondary vacuum and the cooling is performed passively through the metallic layers of the board itself.

There are two possible ways of adding a time-stamp to the recorded protons: a TDC connected with single or multiple threshold discriminators or a high bandwidth signal sampler. The two possibilities considered have slightly different performances: the first gives a better trigger capability, while the second has a better time resolution.

Discriminator and time over threshold measurement with a TDC: each pixel is equipped with a wide bandwidth transconductance preamplifier and the output voltage is proportional to the input current generated from the collected charge that discharges on the input resistance. A single

threshold discriminator detects the edge of the signal. The time walk of a single threshold discriminators, consequence of charge fluctuations, can be corrected measuring the time over threshold for each signal. In this case the signal rise time is limited by the bandwidth and with the present electronics is possible to obtain rise time down to $\sim 180ps$. The criticality of this approach is that for a MIP the signal to noise ratio is lower than 2. A way to improve the S/N is either to add coherently with one preamplifier the signal produced in two (or more) diamond planes connected in parallel or to increase the input resistance of the amplifier as discussed in [58]. However the understanding of both solutions requires a certain amount of simulations and tests.

The NINO chip [59] provides this possibility, the output signal length being proportional to the time over threshold of the input analog signal. The maximum acquisition rate of this device is around 30 MHz which in turn implies an average rate for each pixel of less than 10 MHz, well below the maximum rate expected in the experiment. The front end board for one plane will have 10 LVDS output signals each one providing both the pixel information of time of arrival with the leading edge and the charge released with the signal length.

Digital sampling: the signal from each pixel is integrated and then sampled with a high bandwidth signal sampler. To extract the timing information from the output of a preamplifier with a known transfer function, an appropriate algorithm reconstructs the original signal.

The sampling can be performed with the SAMPIC chip developed in Saclay [60]. The chip has 16 input channels with a sampling rate up to 10 Gs/s which provides a good signal reconstruction, due to the fact that the preamplifier has a rise time of 2ns (see Figure 16).

For each channel a circular buffer of capacitors continuously samples the input signal. Digitization of the buffer using a 11 bit Wilkinson ADC starts either when an external trigger is provided or when the input signals goes above a programmable threshold (see Figure 17 for a diagram of the chip).

A future version of the chip will allow a minimum 50 ns dead time on each independent channel by using a faster interleaved readout between two or four channels and a function to control the internal trigger, for instance start conversion only when the internal trigger fires in coincidence with the bunch crossing, and the possibility of a fast read-out of the internal trigger time-stamp to be complemented with a more precise timing information after the digital analysis of the sampled signal will be completed.

The SAMPIC with a CSA preamplifier has been tested with a pair of "Ultra-Fast" Silicon detectors [61]. Figure 18 shows the time difference measured between the two detectors pulsed with the same laser via an optical splitter and using an off-line algorithm. The resolution achieved on the timing difference is of ~ 40 ps, which indicates a resolution of ~ 30 ps for a single measurement. More studies will follow with diamond detectors in a real test beam or cosmic rays.

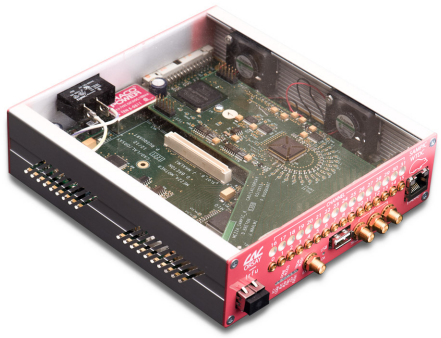

Figure 16: *The board with the SAMPIC chip, developed in Saclay, used for the first tests.*

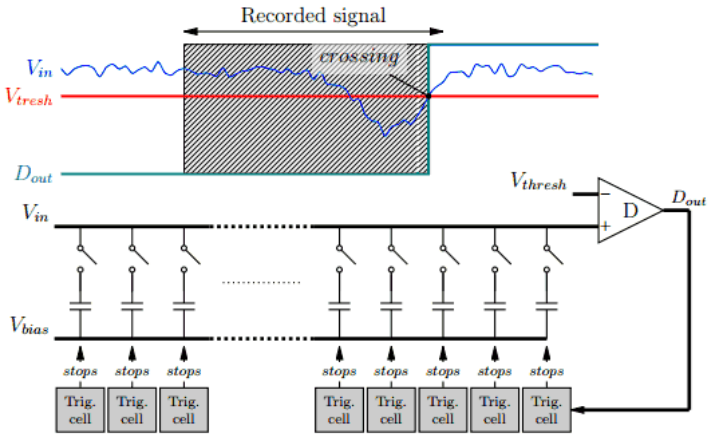

Figure 17: *Inside the SAMPIC, the input signal is continuously sampled in a ring analog buffer. In internal trigger mode, the signal is compared to a programmable threshold to stop the sampling and start the ADC conversion.*

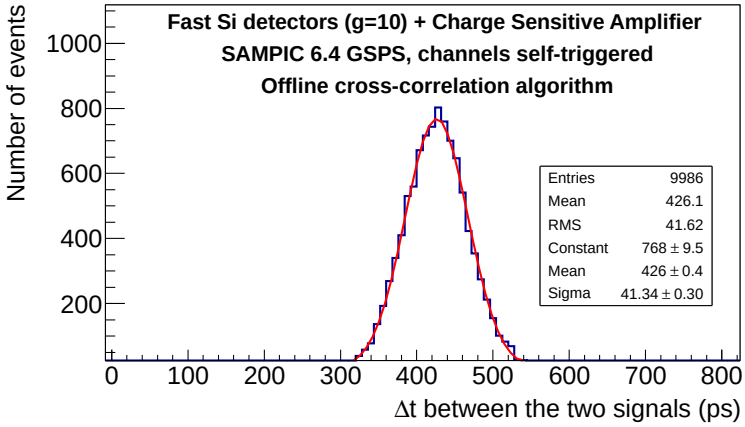

Figure 18: *Distribution of the time difference between two Ultra-Fast Silicon detectors pulsed with the same laser and read with fast CSA and SAMPIC, using an advanced off-line algorithm.*

Preliminary Tests: Two diamond detectors, 0.5x0.5 mm in size and 500 micron in thickness, have been purchased from Cividec Instrumentation[6] together with state of the art CSA and wide-band amplifiers with specs optimized to our request, and assembled in a telescope (Figure 19) for measurements with particles on a test beam (Figure 20). Moreover new transimpedance preamplifiers have been developed in house in order to study and optimise the input impedance of the circuits. Three beam test have been performed in PSI and Cern PS, with different configurations. The detectors where connected to the preamplifiers with SMA connectors. The input capacitance, of about 0.5 pF from the detector, was dominated by the connectors (5-10 pF). The rise time of the signals is strongly affected by this parameter and therefore a reduction in performance is expected. The resolution obtained is around 190 ps, well in line with the expected value, and a dramatic im-

[6]http://www.cividec.at

provement is expected with a design of the hybrid that removes the connector. The final step is therefore to design and bring to a test-beam a hybrid with first-stage preamplifiers bonded as close as possible to the detector, in order to keep the capacitance below $\sim$ 1 pF. A similar design has already been used successfully elsewhere [62]. Construction of the new hybrid has already started.

Other Technical Considerations: A cooling system will be provided for the electronics only, since the diamond detectors do not dissipate any power from the polarization power supply.

All the electronics that need to be as close as possible to the actual detector and that makes use of FPGAs (as the control/transmission board for the SAMPIC or, in alternative, the TDC board) can operate only in regions with reasonable radiation levels. Studies performed on Altera Cyclone FPGA with ion and neutron beams show that even in the surrounding area of the beam pipe we could expect for high luminosity runs a SEU (single event upset) rate of 1 every 3 hours, which is already orders of magnitude higher than what was experienced in the special high beta optics runs. For this reason space close to the Roman Pot station located in the floor of the tunnel will be available to keep the electronics as far possible from the beam pipes. In case of SEU a Resync request will be needed only for the TDC board.

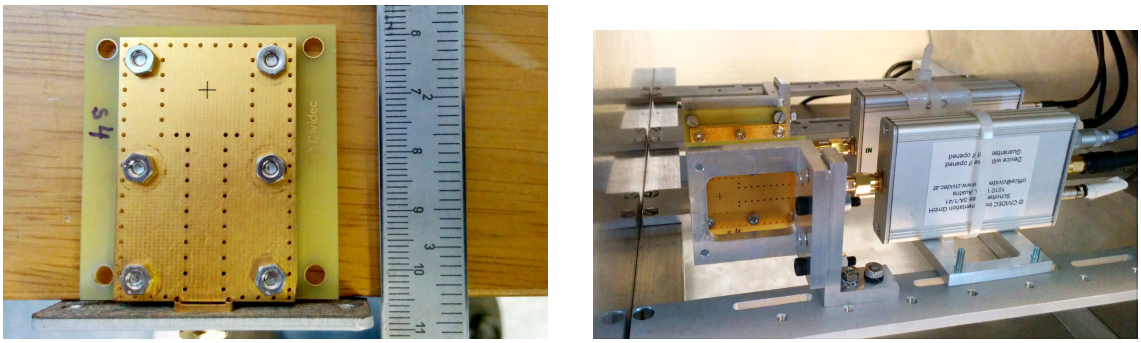

Figure 19: *Prototype of the diamond detector from Cividec Instrumentation (left) and the assembly of the test telescope (right).*

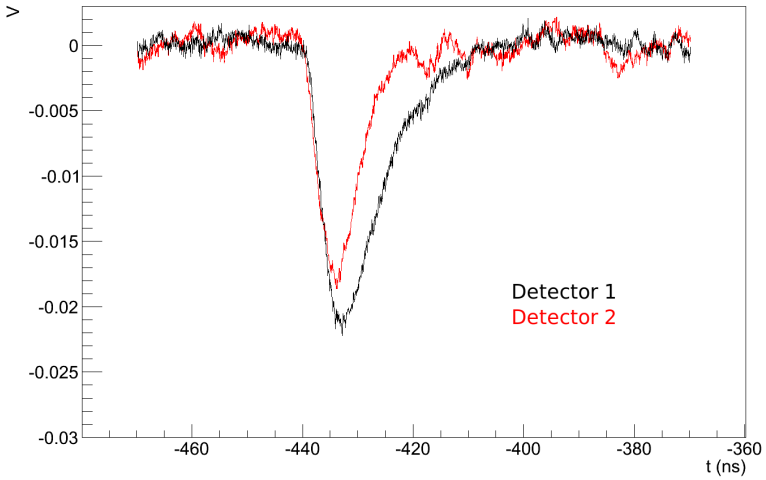

Figure 20: *Signals of two diamond detectors read with a fast Charge Sensitive Amplifier in a test beam measurent with 12 GeV π^-.*

TDCs with a time resolution of ∼10ps inside an FPGA are in advanced stage of development by TOTEM, and are under evaluation. The time reconstruction algorithm measures the crossing time for a single threshold and the time over threshold and a correction matrix. In case we will use the SAMPIC chip, the data have to be fitted in a simple FPGA board. The advantage of using on board FPGAs is that the Trigger and DAQ information will be formatted on the same board. The event is formatted for DAQ with a header, a start of frame patterns and counters, the list of TOA (Time Of Arrival) and TOT (Time Over Threshold) for each fired pixel, and a footer. The information is transmitted without on-line corrections.

The Trigger algorithm instead will perform an on-line rejection on the number of tracks (see Section 4.2.2). In order to filter out noisy channels that could contaminate the time measurement a trigger signal (a track road) is generated only if the signals from aligned pixels from adjacent planes satisfy a majority-AND condition. Track counting is done locally and, if the event is accepted, the time of arrival is formatted into 4 words and sent to the central trigger unit (Totem LONEG board).

5.2 Clock distribution

The challenge of combining measurements with picosecond range precision for Timing signals generated in locations separated by large distances (order of 220 m) requires a clock distribution system capable of the highest precision and of the utmost time stability.

The following pages aim at describing the Clock Distribution system for the TOTEM Timing Upgrade. The system is adapted from the *Universal Picosecond Timing System* [62], developed for FAIR (Facility for Antiproton and Ion Research), the new, unique international accelerator facility for research with antiprotons and ions presently under construction at GSI (D), where a Bunch phase Timing System (BuTiS) based on this concept has been implemented [63].

The optical clock distribution network will use a Dense Wavelength Division Multiplex (DWDM) technique that makes it possible to transmit multiple signals of different wave-lengths over a common single mode fibers. This will allow to use standard telecommunication modules compliant to ITU (International Telecommunications Union) international standards.

The experiment requires two very stable clocks for the precise timing reference of the measurement and the bunch identification. These reference clock signals are sent from the counting room to a set of receivers positioned near the timing detectors in various location of the LHC tunnel on both sides of IP5. A third signal added on the same optical fiber will be simply reflected back to be used to continuously measure the time delay of each optical transmission line: these delay measurements are necessary to correct the time information generated at the detector location for fiber delay variations (thermal and mechanical instabilities).

The system can be logically subdivided in four major blocks: the Transmission Unit, the Distribution Unit, the Measurement Unit and the Receiving Unit. One Receiving Unit must be installed very near each Roman Pot location, the Transmission, Distribution and Measurement Units will be located in the TOTEM racks in the IP5 counting room. A block diagram of the entire system is reproduced in Figure 21.

Measurements performed with the prototype of the "BuTiS" system show that the influence of the transmission system on the signal jitter, is of the order of 0.4 ps [63], mainly dependent on the quality of the clock source signal, the noise added by the optical components and the bandwidth of the transmission system itself. Using a transmission system based on this concept, the total jitter of the TOTEM clock transmission system will also be due mainly to the inherent jitter of clock sources and the end user electronics.

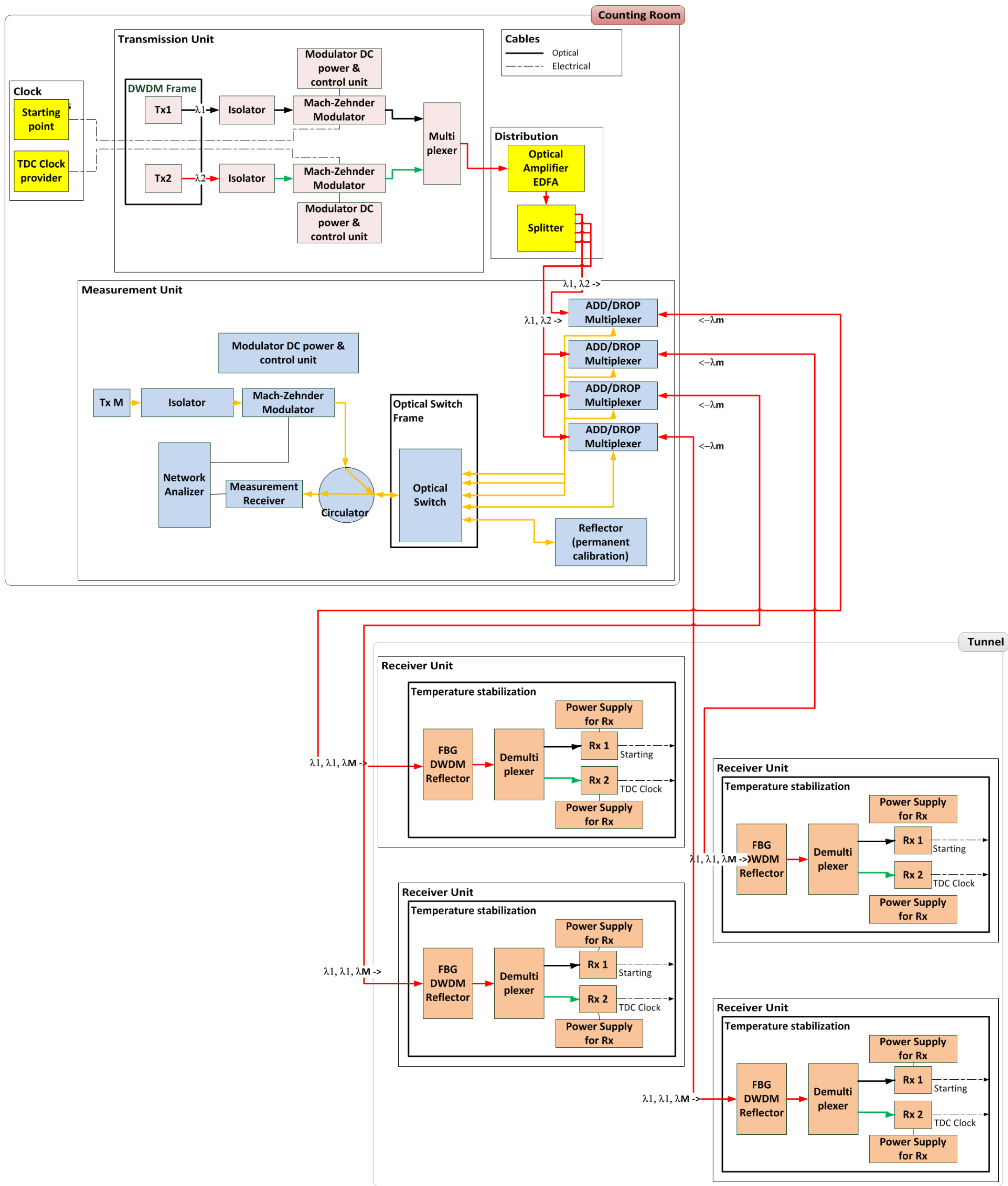

Figure 21: *The clock distribution system*

5.2.1 Transmission Unit

The Transmission Unit optically modulates the two reference clocks in signals with different wavelength λ_1 and λ_2. Via DWDM these optical signal are multiplexed into a single fiber and re-transmitted at a specific wavelength using a 1,550 nm band laser to the Distribution Unit. The signal is amplified with an erbium-doped fiber amplifier (EDFA) to compensate the attenuation due to further splitting and the multiplexers.

A Thorlabs PRO8000[7] platform has been chosen to generate the two DWDM wavelengths on channels ITU 32 and ITU 34 . This complete platform is designed to operate and control electrical

[7]Thorlabs, Inc. : www.thorlabs.com. PRO8000 platform: http://www.thorlabs.com/newgrouppage9.cfm?objectgroup_id=895
.

and optical modules for telecommunication testing and application developments from a broad family of interchangeable modular devices and can be controlled by an external computer using industrial control protocols. The modulation of the optical signals is performed by two military grade Mach-Zehnder modulators with a 20GHz bandwidth. This unit can be rack mounted and is suitable for use in the experiment control room harsh environment.

5.2.2 Distribution Unit

The DWDM optical signal, as generated by the Transmission Unit, needs to be split in order to be transmitted to the four Receiving Units. Moreover a third DWDM modulated optical signal of wavelength λ_M is needed to measure the transmission delays over each fiber and is added to the other two clock signals.

The JDSU[8] Multiple Application Platform (MAP-200) has been chosen for the Distribution Unit optical amplification, optical signal splitting and switching. This platform is a highly configurable, scalable and industrially controlled system that can host several optical modules with a wide range of functions. The EDFA amplifier developed for this platform will be used for the signal optical amplification.

5.2.3 Measurement Unit

The signals' delay are measured in this unit. A reference signal is generated, optically modulated using the wavelength λ_M and sent via an optical switch to every Receiving Unit and to a reflector, which will be used for calibration.

Add/drop multiplexers combine this reference signal to each of the 4 DWDM optical signals generated in the Transmission Unit and split in the Distribution Unit. The multiplexed signal, that now contains the three modulated optical wavelengths: λ_1, λ_2 and λ_M, is transmitted to the Receiving Units located in the tunnel at $\pm$220m and $\pm$210m.

The λ_M optical reference signal once at the Receiving Unit is reflected back to the Measurement Unit, where the optical add/drop multiplexer separates the λ_M optical signal coming back from the RUs and pass it back to the optical switch. A "circulator", placed between the DWDM modulator and the switch, distributes the reflected signals to a measurement instrument without interrupting the transmission from the generation module to the switch. A phase comparison of the reflected signal with the reference one is performed, using a vector network analyzer. The phase differences obtained by this measurement determine the delay of each clock signal distribution channel.

As for the Transmission Unit, a Thorlab PRO8000 module, and the same Mach-Zender modulator, will be used. The DWDM wavelengths proper of channel ITU 36, will be used to modulate the reference signal.

5.2.4 Receiving Unit

The Receiving Unit separates the multi-wavelength optical signal at the RP stations into individual signals.

The signal from the single mode fiber (SMF) encounters first a Bragg grating (FBG) DWDM reflector and reflects back the signal component of λ_M wavelength. The other components of the signal are routed to a DWDM demultiplexer that separates the two wavelengths, λ_1 and λ_2, and outputs them on separate fibers for conversion to electrical signals and delivered to the front end electronics and DAQ cards eventually.

[8]JDS Uniphase Corporation: www.jdsu.com. Multiple Application Platform (MAP-200): http://www.jdsu.com/en-us/test-and-measurement/products/a-z-product-list/Pages/map.aspx .

This unit should be located as close as possible to every Roman Pot location. A temperature stabilization of this unit, depending on the temperature characterization of the installation point in the tunnel, may be needed to reduce the long term shift of the measured delay.

6 Costs and Schedule

6.1 Costs

The cost sharing among the TOTEM Collaboration Institutions is described in Table 7.

Table 7: *Estimated costs of the TOTEM timing upgrade in the Vertical RP and related contributions from the TOTEM Institutions.*

TOTEM Timing Upgrade - Vertical RP - Costs in kCHF (Spent, Committed, Allocated for the years 2013-2016)											
Work Package	CERN			INFN			Finland			Czech	**TOTAL**
RP relocation	70	140									210
RP rotation	10										10
RP new ferrites	10	10									20
Clock distribution R&D				14							14
Clock distribution						160					160
Timing detector R&D		20	50	46							141
Timing detetector infrastructure				30		60					90
Timing detectors (vertical RP)			100			110		50	100		335
TOTAL	90	170	150	90		330		50	100		980

6.2 Schedule

The final phase of the design and construction of the Time Of Flight (TOF) apparatus will start in Jan 2015.

before installation in the LHC each detector will thoroughly be tested with a particle beam in our setup in the North Area (H8) . A first milestone sees, preliminary to the full installation, a complete full detector mounted in the experiment in the September 2015 LHC technical stop for tests.

Considering the experience gained from this detector, the full detector will be then installed in the 2015-2016 winter shut-down.

The small additions to the infrastructure in the LHC tunnel necessary for the experiment upgrade have been already done during LS1.

The clock distribution system will be assembled and tested during the machine technical stops before the end of August 2015, so as to be ready for the arrival of the first detector in September 2015.

The detailed schedule is reproduced in Figure 22.

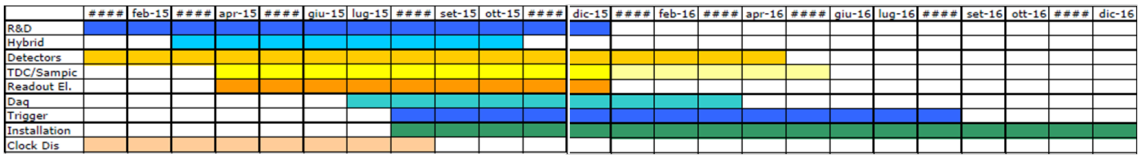

Figure 22: *Timetable for the construction and installation of the TOTEM TOF detectors in the Vertical Pots.*

References

[1] G. Antchev *et al.* (TOTEM Collaboration), "Proton-proton elastic scattering at the LHC energy of $\sqrt{s} = 7$ TeV", Europhys.Lett. **95** (2011) 41001.

[2] G. Antchev *et al.* (TOTEM Collaboration), "First measurement of the total proton-proton cross section at the LHC energy of $\sqrt{s} = 7$ TeV", Europhys.Lett. **96** (2011) 21002.

[3] G. Antchev *et al.* (TOTEM Collaboration), "Luminosity-independent measurements of total, elastic and inelastic cross-sections at $\sqrt{s} = 7$ TeV", Europhys.Lett. **101** (2013) 21004.

[4] G. Antchev *et al.* (TOTEM Collaboration), "Measurement of proton-proton elastic scattering and total cross-section at $\sqrt{s} = 7$ TeV", Europhys.Lett. **101** (2013) 21002.

[5] G. Antchev *et al.* (TOTEM Collaboration), "A luminosity-independent measurement of the proton-proton total cross-section at $\sqrt{s} = 8$ TeV", Phys. Rev. Lett. **111** (2013) 012001.

[6] G. Antchev *et al.* (TOTEM Collaboration), "Measurement of proton-proton inelastic scattering cross-section at $\sqrt{s} = 7$ TeV", Europhys.Lett. **101** (2013) 21003.

[7] G. Antchev *et al.* (TOTEM Collaboration), "Double diffractive cross-section measurement in the forward region at LHC", Phys. Rev. Lett. **111** (2013) 262001.

[8] G. Antchev *et al.* (TOTEM Collaboration), "Measurement of the forward charged-particle pseudorapidity density in pp collisions at $\sqrt{s} = 7$ TeV with the TOTEM experiment", Europhys.Lett. **98** (2012) 31002.

[9] S. Chatrchyan *et al.* (CMS and TOTEM Collaborations), "Measurement of pseudorapidity distributions of charged particles in proton-proton collisions at $\sqrt{s}$ = 8 TeV by the CMS and TOTEM experiments", CMS-FSQ-12-026, CERN-PH-EP-TOTEM-2014-002, CERN-PH-EP-2014-063 (2014).

[10] V. Berardi *et al.* (TOTEM Collaboration), "Total cross-section, elastic scattering and diffraction dissociation at the Large Hadron Collider at CERN: TOTEM technical design report", CERN-LHCC-2004-002 and addendum CERN-LHCC-2004-020 (2004).

[11] The TOTEM collaboration, "TOTEM upgrade proposal", CERN-LHCC-2013-009 / LHCC-P-007 (2013).

[12] The CMS and TOTEM diffractive and forward physics working group, "Prospects for Diffractive and Forward Physics at the LHC", CERN/LHCC 2006-039/G-124 (2006).

[13] V.A. Khoze, A.D. Martin, and M.G. Ryskin, "Double-diffractive processes in high-resolution missing-mass experiments at the Tevatron", Eur. Phys. J. **C 19** (2001) 477 and erratum ibid. **C 20** (2001) 599.

[14] The CMS and TOTEM Collaborations, "CMS-TOTEM Precision Proton Spectrometer", CERN-LHCC-2014-021; CMS-TDR-13; TOTEM-TDR-003 (2014).

[15] V. Matheiu, N. Kochelev and V.Vento, "The physics of glueballs", Int J. Mod. Phys. **E 18** (2009) 1.

[16] Y. Chen *et al.*, "Glueball spectrum and matrix elements on anisotropic lattices", Phys. Rev. **D 73** (2006) 014516.

[17] W. Ochs, "The status of glueballs", J. Phys. **G 40** (2013) 043001.

[18] T. Åkeson *et al.* (Axial Field Spectrometer Collaboration), "A Search for Glueballs and a Study of Double Pomeron Exchange at the CERN Interacting Storage Rings", Nucl. Phys. **B 264** (1986) 154.

[19] A. Breakstone *et al.* (Ames-Bologna-CERN-Dortmund-Heidelberg-Warsaw Collaboration), "Production of the f^0 meson in Double Pomeron Exchange reaction $pp \to pp\pi^+\pi^-$ at $\sqrt{s}$ = 62 GeV", Z. Phys. **C 31** (1986) 185.

[20] J. Turnau on behalf of STAR collaboration, "Measurement of the Central Exclusive Production of pion pairs using tagged forward protons at the STAR detector at RHIC", PoS DIS2014 (2014) 098.

[21] M. Albrow, A. Swiech and M. Zurek on behalf of CDF collaboration, "Exclusive Central $\pi^+\pi^-$ production in CDF", FERMILAB-CONF-13-467-PPD (2013), arXiv:1310.3839.

[22] A. Kirk, "Resonance production in central pp collisions at the CERN Omega Spectrometer", Phys. Lett **B 489** (2000) 29.

[23] M. G. Albrow, T. D. Coughlin and J. R. Forshaw, "Central exclusive particle production at high energy hadron colliders", Prog. Part. Nucl. Phys. **65** (2010) 149, arXiv:1006.1289.

[24] L.A. Harland-Lang, V.A. Khoze, M.G. Ryskin and W.J. Stirling, "Standard candle central exclusive processes at the Tevatron and LHC", Eur. Phys. J. **C 69** (2010) 179.

[25] T. Aaltonen *et al.* (CDF Collaboration), "Observation of Exclusive Charmonium Production and $\gamma\gamma \to \mu^+\mu^-$ in $p\bar{p}$ Collisions at $\sqrt{s}$ = 1.96 TeV", Phys. Rev. Lett. **102** (2009) 242001.

[26] LHCb Collaboration, "Central Exclusive Dimuon Production at $\sqrt{s}$ = 7 TeV", LHCb-CONF-2011-022 (2011).

[27] R.S. Pasechnik, A. Szczurek and O.V. Teryaev, "Diffractive production of $\chi_c(0^+, 1^+, 2^+)$ mesons at LHC, Tevatron and RHIC", PoS EPS-HEP2009 (2009) 335, arXiv:0909.4498.

[28] R. Aaij *et al.* (LHCb Collaboration), "Updated measurements of exclusive J/Ψ and $\Psi(2S)$ production cross-sections in pp collisions at $\sqrt{s}$ = 7 TeV", J. Phys. **G 41** (2014) 055002.

[29] B.B. Abelev *et al.* (Alice Collboration), "Exclusive J/Ψ photoproduction off protons in ultra-peripheral p-Pb collisions at $\sqrt{s_{NN}}$ = 5.02 TeV", CERN-PH-EP-2014-149 (2014), arXiv:1406.7819.

[30] R. Aaij *et al.* (LHCb Collaboration), "Observation of charmonium pairs produced exclusively in pp collisions", CERN-PH-EP-2014-174 (2014), arXiv:1407.5973.

[31] L. Motyka, "Searching for odderon in exclusive vector meson hadroproduction", Proceedings of DIS2008 (2008), arXiv:0808.2216.

[32] H. Niewiadomski on behalf of TOTEM collaboration, "TOTEM Physics program, analysis and results", LHC seminar 29 January 2013, `http://indico.cern.ch/event/230889/`.

[33] T. Aaltonen *et al.* (CDF Collaboration), "Observation of exclusive dijet production at the Fermilab Tevatron $p\bar{p}$ collider", Phys. Rev. **D 77** (2008) 052004.

[34] V.A. Khoze, M.G. Ryskin and W.J. Stirling, "On radiative QCD backgrounds to exclusive $H \to b\bar{b}$ production at the LHC and a photon collider", Eur. Phys. J. **C 48** (2006) 477.

[35] L.A. Harland-Lang, V.A. Khoze, M.G. Ryskin and W.J. Stirling, "Central exclusive production within the Durham model: a review", Int.J.Mod.Phys. **A 29** (2014) 1430031, arXiv:1405.0018.

[36] V.A. Petrov and R.A. Ryutin, "Patterns of the exclusive double diffraction", J. Phys. G **35** (2008) 065004; R.A. Ryutin, "Exclusive double diffractive events: general framework and prospects", Eur. Phys. J. **C 73** (2013) 2443.

[37] C. Marquet, C. Royon, M. Saimpert and D. Werder, "Probing the Pomeron structure using dijets and γ+jet events at the LHC", Phys. Rev. **D 88** (2013) 074029.

[38] H. Burkhardt, *private communication*.

[39] G. Antchev *et al.* (TOTEM Collaboration), "The TOTEM Experiment at the CERN Large Hadron Collider", JINST **3** (2008) S08007.

[40] G. Antchev *et al.* (TOTEM Collaboration), "Performance of the TOTEM detectors at the LHC", Int. J. Mod. Phys. A **28** (2013) 1330046.

[41] G. Antchev *et al.* (TOTEM Collaboration), "LHC Optics Measurement with Proton Tracks Detected by the Roman Pots of the TOTEM Experiment", arXiv:1406.0546, *accepted for publication by NJP*.

[42] H. Niewiadomski, "Reconstruction of Protons in the TOTEM Roman Pot Detectors at the LHC", Ph.D. thesis, University of Manchester 2008, CERN-THESIS-2008-080.

[43] R. Engel, Z. Phys. C, **66** (1995) 203; R. Engel and J. Ranft, Phys. Rev. **D54** (1996) 4244.

[44] M. Mannelli *et al.*, "The CMS tracker system project: Technical Design Report", CERN-LHCC-98-006 (1997)

[45] S. Chatrchyan *et al.* (CMS Collaboration), "The CMS experiment at the CERN LHC", JINST **3** (2008) S08004.

[46] F. Siklèr (for CMS Collaboration), "Low p_T Hadronic Physics with CMS", Int. J. Mod. Phys. E**16** (2007) 1819-1825.

[47] S. Chatrchyan *et al.* (CMS Collaboration), "Study of the inclusive production of charged pions, kaons, and protons in pp collisions at $\sqrt{s}$ = 0.9, 2.76, and 7 TeV", Eur. Phys. J. **C 72** (2012) 2164.

[48] S. Chatrchyan *et al.* (CMS Collaboration), "Study of the production of charged pions, kaons, and protons in pPb collisions at $\sqrt{s_{NN}}$ = 5.02 TeV", Eur. Phys. J. **C 74** (2014) 2847.

[49] F. Siklér (for CMS Collaboration), "A parametrization of the energy loss distributions of charged particles and its applications for silicon detectors", Nucl. Inst. and Meth.**A 691** (2012) 16–29.

[50] S. Chatrchyan *et al.* (CMS Collaboration), "Description and performance of track and primary-vertex reconstruction with the CMS tracker", CERN-PH-EP-2014-070, Submitted to JINST.

[51] F. Siklèr (for CMS Collaboration), "Study of clustering methods to improve primary vertex finding for collider detectors", Nucl. Instr. and Meth. in Phys. R. **A621** (2010) 526–533.

[52] G. Aad *et al.* (ATLAS Collaboration), "Charged-particle multiplicities in pp interactions measured with the ATLAS detector at the LHC", New J. Phys. **13** 053033, 2011.

[53] T. Sjostrand, S. Mrenna, P. Skands, JHEP **0605** (2006) 026, hep-ph/0603175.

[54] P. Bruni and G. Ingelman, Phys. Lett. **B311**, 317 (1993).

[55] M. Trzebinski, "Study of QCD and Diffraction with the ATLAS detector at the LHC", CERN THESIS-2013-166, page 136.

[56] M. Berretti, "Performance studies of the Roman Pot timing detectors in the forward region of the IP5 at LHC", CERN-TOTEM-NOTE-2014-001 (2014).

[57] M. Albrow *et al.*, "Quartz Cherenkov counters for fast timing: QUARTIC", Journal of Instrumentation **7** (2012) P10027.

[58] M. Osipenko *et al.*, "Comparison of Fast Amplifiers for Diamond Detectors", arXiv:1310.1000 (2013).

[59] F. Anghinolfi *et al.*, "NINO: an ultra-fast and low-power front-end amplifier/discriminator ASIC designed for the multigap resistive plate chamber", Nucl. Inst. and Meth.**A** 533 (2004) 183–187.

[60] H. Grabas, "Developing Picosecond Time of Flight detectors", PhD Thesis - Université Paris Sud - (2013).

[61] N. Cartiglia *et al.*, "Performance of Ultra-Fast Silicon Detectors", arXiv:1312.1080 (2013).

[62] M. Bousonville and J. Rausch, "Universal picosecond timing system for the Facility for Antiproton and Ion Research", Phys. Rev. ST Accel. Beams **12** (2009) 042801.

[63] P. Moritz and B. Zipfel, "Recent Progress on the Technical Realization of the Bunch Phase Timing System BuTiS", IPAC-2011-MOPC145 Conf.Proc. C110904 (2011) 418-420.